Analytic continuation over complex landscapes

Jaron Kent-Dobias[*] and **Jorge Kurchan**

Laboratoire de Physique de l'Ecole Normale Supérieure, Paris, France

E-mail: jaron.dobias@phys.ens.fr

Abstract

In this paper we follow up the study of 'complex complex landscapes' (Kent-Dobias and Kurchan 2021 *Phys. Rev. Res.* **3** 023064), rugged landscapes of many complex variables. Unlike real landscapes, the classification of saddles by index is trivial. Instead, the spectrum of fluctuations at stationary points determines their topological stability under analytic continuation of the theory. Topological changes, which occur at so-called Stokes points, proliferate among saddles with marginal (flat) directions and are suppressed otherwise. This gives a direct interpretation of the gap or 'threshold' energy—which in the real case separates saddles from minima—as the level where the spectrum of the hessian matrix of stationary points develops a gap. This leads to different consequences for the analytic continuation of real landscapes with different structures: the global minima of 'one step replica-symmetry broken' landscapes lie beyond a threshold, their hessians are gapped, and are locally protected from Stokes points, whereas those of 'many step replica-symmetry broken' have gapless hessians and Stokes points immediately proliferate. A new matrix ensemble is found, playing the role that GOE plays for real landscapes in determining the topological nature of saddles.

Keywords: random landscapes, analytic continuation, *p*-spin models

(Some figures may appear in colour only in the online journal)

[*] Author to whom any correspondence should be addressed.

Contents

1. Introduction

Complex landscapes are functions of many variables having many minima and, inevitably, many saddles of all indices (their number of unstable directions). Optimization attempts to find the deepest minima, often a difficult task. For example, particles with a repulsive mutual potential enclosed in a box will have many stable configurations, and we are asked to find the one with lowest energy.

An aim of complexity studies is to classify these landscapes into families having common properties. Two simplifications make the task potentially tractable. The first is to consider the limit of many variables; in the example of the particles, the limit of many particles, i.e. the thermodynamic limit. The second simplification is of a more technical nature: we often consider functions that contain some random element to them, and we study the ensemble average over that randomness. The paradigm of this are spin-glasses, where the interactions are random, and we are asked to find the ground state energy for typical samples.

Spin glass theory gave a surprise: random landscapes come in two kinds. The first kind have a 'threshold level' of energy, below which there are many minima but almost no saddles, resulting in low minima that are separated by high barriers. The second have all sorts of saddles all the way down to the lowest energy levels, and local minima are separated by barriers of sub-extensive energy height. The latter are still complex, but good solutions are easier to find. This classification is closely related to the structure of their replica trick solutions, the former being 'one step replica-symmetry broken' and the latter being 'many step replica-symmetry broken.' Armed with this solvable random example, it was easy to find non-random examples that behave (at least approximately) in these two ways. For example, sphere packings and the traveling salesman problem belong to first and second classes, respectively.

What about the classification of systems whose variables are not real, but rather, complex? Recalling the Cauchy–Riemann conditions, one finds a difficulty: if our cost is, say, the real part of a function of N complex variables, in terms of the corresponding $2N$ real variables it has only saddles of index N. Even worse: often not all saddles are equally interesting, so simply finding the lowest is not usually what we need to do. As it turns out, there is a set of interesting questions to ask, as we describe below. For each saddle, there is a 'thimble' spanned by the lines along which the cost function decreases. The way in which these thimbles fill the complex space is crucial for many problems of analytic continuation, and is thus what we need to study. The central role played by saddles in a real landscape, the 'barriers', is now played by the Stokes lines, by which thimbles exchange their properties. Perhaps not surprisingly, the two classes of real landscapes described above retain their significance in the complex case, but the distinction is now that while in the first class the Stokes lines among the lowest minima are rare, in the second class they proliferate.

In this paper we shall start from a many-variable integral of a real function, and deform it in the many variable complex configuration space. The landscape one faces occupies the entirety of this space, and we shall see that this is an example where the proliferation—or lack of it—of Stokes lines is the interesting quantity in this context.

As for analytic continuation of physical theories: it is sometimes useful. Some theories have a well-motivated Hamiltonian or action that nevertheless results in a divergent partition function, and can only be properly defined by continuation from a parameter regime where everything is well-defined [1]. Others result in oscillatory configuration space measures that spoil the use of Monte Carlo or saddle point techniques, but can be treated in a regime where the measure does not oscillate and the results continued to the desired model [2].

In any case, the nicest modern technique (which we will describe in some detail) consists of deforming the configuration space integral into a complex configuration space and then breaking it into pieces associated with stationary points of the action. Each of these pieces, known as *thimbles*, has wonderful properties that guarantee convergence and prevent oscillations. Once such a decomposition is made, analytic continuation is mostly easy, save for instances where the thimbles interact, which must be accounted for.

When your action has a manageable set of stationary points, this process is often tractable. However, many actions of interest are complex, having many stationary points with no simple symmetry relating them, far too many to individually track. Besides appearing in classical descriptions of structural and spin glasses, complex landscapes have recently become important objects of study in the computer science of machine learning, the condensed matter theory of strange metals, and the high energy physics of black holes. What becomes of analytic continuation under these conditions?

2. Analytic continuation by thimble decomposition

2.1. Decomposition of the partition function into thimbles

Consider an action $\mathcal{S}$ defined on the (real) configuration space Ω. A typical calculation stems from a configuration space average of some observable $\mathcal{O}$ of the form:

$$\langle \mathcal{O} \rangle = \frac{1}{Z} \int_{\Omega} ds \, e^{-\beta \mathcal{S}(s)} \mathcal{O}(s), \tag{1}$$

where the partition function Z normalizes the average as:

$$Z = \int_{\Omega} ds \, e^{-\beta \mathcal{S}(s)}. \tag{2}$$

Rather than focus on any specific observable, we will study the partition function itself, since it exhibits the essential features.

We've defined Z in a way that suggests application in statistical mechanics, but everything here is general: the action can be complex- or even imaginary-valued, and Ω could be infinite-dimensional. In typical contexts, Ω will be the euclidean real space $\mathbb{R}^N$ or some subspace of this like the sphere S^{N-1} (as in the p-spin spherical models on which we will treat later). In this paper we will consider only analytic continuation of the parameter β, but any other parameter would work equally well, e.g. of some parameter inside the action. The action for real β will have some stationary points in the real configuration space, i.e. minima, maxima, saddles, and the set of those points in Ω we will call Σ_0, the set of real stationary points. An example action used throughout this section is shown in figure 1.

In order to analytically continue equation (2), $\mathcal{S}$ must have an extension to a holomorphic function on a larger complex configuration space $\tilde{\Omega}$ containing Ω. In many cases this is accomplished by noticing that the action is some sum or product of holomorphic functions, e.g. polynomials, and replacing its real arguments with complex ones. For $\mathbb{R}^N$ the complex configuration space $\tilde{\Omega}$ is $\mathbb{C}^N$, while for the sphere S^{N-1} it takes a little more effort. S^{N-1} can be defined by all points $x \in \mathbb{R}^N$ such that $x^T x = 1$. A complex extension of the sphere is made by extending this constraint: all points $z \in \mathbb{C}^N$ such that $z^T z = 1$. Both cases are complex manifolds, since they are defined by holomorphic constraints, and therefore admit a hermitian metric and a symplectic structure. In the extended complex configuration space, the action often has more stationary points. We'll call Σ the set of *all* stationary points of the action, which naturally contains the set of *real* stationary points Σ_0.
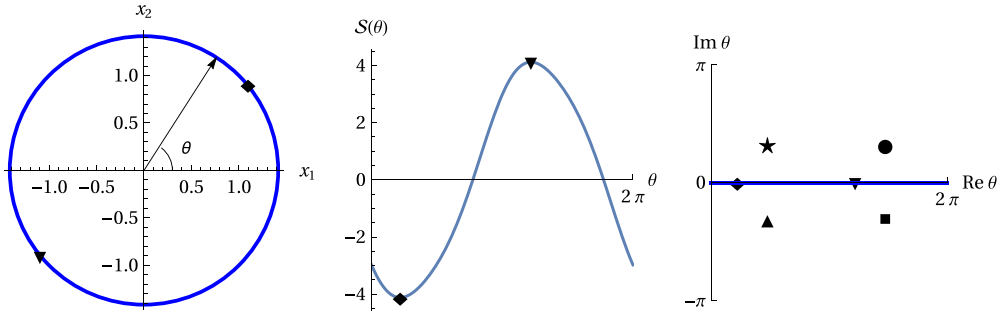
Figure 1. An example of a simple action and its stationary points. Left: the config-
uration space of the $N = 2$ spherical (or circular) model, defined for $x \in \mathbb{R}^N$ restric-
ted to the circle $N = x^T x$. It can be parameterized by one angle $\theta = \arctan(x_2/x_1)$. Its
natural complex extension takes instead $z \in \mathbb{C}^N$ restricted to the hyperbola $N = z^T z =$
$\|\operatorname{Re} z\|^2 - \|\operatorname{Im} z\|^2$. The (now complex) angle θ is still a good parameterization of con-
figuration space. Center: an action $\mathcal{S}$ for circular 3-spin model, defined by $\mathcal{S}(z_1, z_2) =$
$-1.051z_1^3 - 1.180z_1^2 z_2 - 0.823z_1 z_2^2 - 1.045z_2^3$, plotted as a function of θ. Right: the sta-
tionary points of $\mathcal{S}$ in the complex-θ plane. In this example, $\{\blacklozenge, \bigstar, \blacktriangle, \blacktriangledown, \bullet, \blacksquare\}$ and
$\{\blacklozenge, \blacktriangledown\}$. Symmetries exist between the stationary points both as a result of the conjug-
ation symmetry of $\mathcal{S}$, which produces the vertical reflection, and because in the pure
3-spin models $\mathcal{S}(-z) = -\mathcal{S}(z)$, which produces the simultaneous translation and inver-
sion symmetry.

Assuming $\mathcal{S}$ is holomorphic (and that the configuration space Ω is orientable, which is
usually true) the integral in equation (2) can be considered an integral over a contour in the
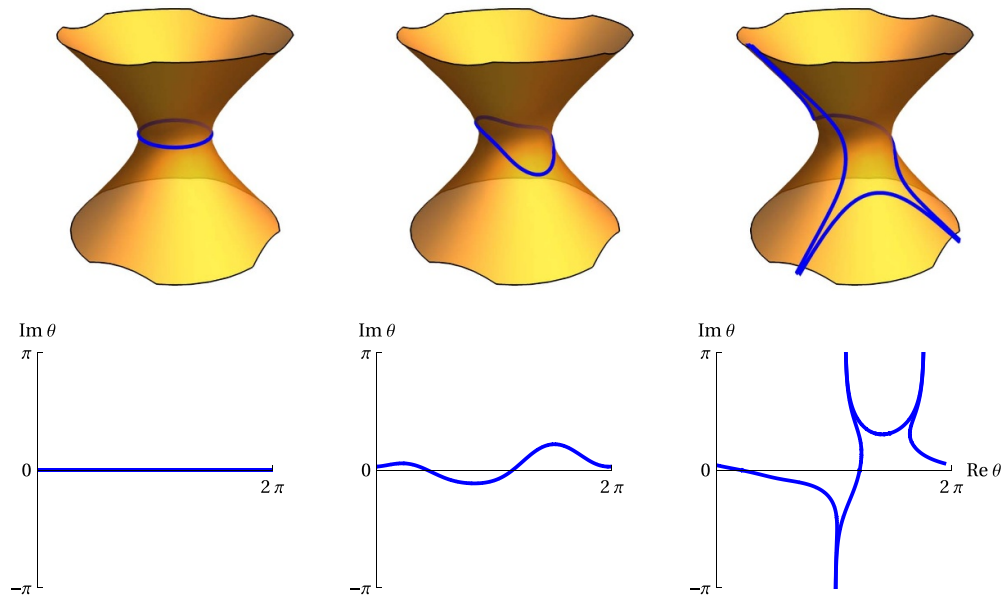complex configuration space $\tilde{\Omega}$, or:

$$Z = \oint_{\tilde{\Omega}} ds \, e^{-\beta \mathcal{S}(s)}. \tag{3}$$

For the moment this translation has only changed a symbol from equation (2), but concep-
tually it is important: contour integrals can have their contour freely deformed (under some
constraints) without changing their value. This means that we are free to choose a nicer contour
than our initial configuration space Ω. This is illustrated in figure 2.

What properties are desirable for our contour? Consider the two motivations for perform-
ing analytic continuation cited in the introduction: we want our partition function to be well-
defined, i.e. for the configuration space integral to converge, and we want to avoid oscillations
in the phase of the integrand. The first condition, convergence, necessitates that the real part
of the action $\operatorname{Re} \beta \mathcal{S}$ be bounded from below, and that it approach infinity in any limiting dir-
ection along the contour. The second, constant phase, necessitates that the imaginary part of
the action $\operatorname{Im} \beta \mathcal{S}$ be constant.

Remarkably, there is an elegant recipe for accomplishing both these criteria at once, cour-
tesy of Picard–Lefschetz theory. For a more thorough review, see [1]. We will construct our
deformed contour out of a collection of pieces called *thimbles*. There is one thimble $\mathcal{J}_\sigma$ asso-
ciated with each of the stationary points $\sigma \in \Sigma$ of the action, and it is defined by all points that
approach the stationary point s_σ under gradient descent on $\operatorname{Re} \beta \mathcal{S}$: each thimble is the basin
of attraction of a saddle.

Thimbles guarantee convergent integrals by construction: the value of $\operatorname{Re} \beta \mathcal{S}$ is bounded
from below on the thimble $\mathcal{J}_\sigma$ by its value $\operatorname{Re} \beta \mathcal{S}(s_\sigma)$ at the stationary point, since all other
points on the thimble must descend to reach it. And, as we will see in the following subsection,

Figure 2. A schematic picture of the complex configuration space for the circular p-spin model and its standard integration contour. Top: for real variables, the model is a circle, and its analytic continuation is a kind of complex hyperbola, here shown schematically in three dimensions. Bottom: since the real manifold (the circle) is one-dimensional, the complex manifold has one complex dimension, here parameterized by the angle θ on the circle. Left: the integration contour over the real configuration space of the circular model. Center: complex analysis implies that the contour can be freely deformed without changing the value of the integral. Right: a funny deformation of the contour in which pieces have been pinched off to infinity. So long as no poles have been crossed, even this is legal.

thimbles guarantee constant phase for the integrand as well, a result of the underlying complex geometry of the problem.

What thimbles are necessary to reproduce our original contour, Ω? The answer is, we need the minimal set which produces a contour between the same places. Simply stated, if $\Omega = \mathbb{R}$ produced a configuration space integral running along the real line from left to right, then our contour must likewise go continuously from left to right, perhaps with detours to well-behaved places at infinity (see figure 3). The less simply stated versions follows.

Let $\tilde{\Omega}_T$ be the set of all points $z \in \tilde{\Omega}$ such that $\operatorname{Re} \beta \mathcal{S}(z) \geqslant T$, where we will take T to be a very large number. $\tilde{\Omega}_T$ contains the parts of the manifold where it is safe for any contour to end up if its integral is to converge, since these are the places where the real part of the action is very large and the real part of the integrand vanishes exponentially. The relative homology group $H_N(\tilde{\Omega}, \tilde{\Omega}_T)$ describes the homology of N-dimensional cycles which begin and end in Ω_T, i.e. are well-behaved. Therefore, any well-behaved cycle must represent an element of $H_N(\tilde{\Omega}, \tilde{\Omega}_T)$. In order for our collection of thimbles to produce the correct contour, the composition of the thimbles must represent the same element of this relative homology group.

Each thimble represents an element of the relative homology, since each thimble is a contour on which the real part of the action diverges at its extremes. And, thankfully for us, Morse theory on our complex manifold $\tilde{\Omega}$ implies that the set of all thimbles produces a basis for this relative homology group, and therefore any contour can be represented by some composition
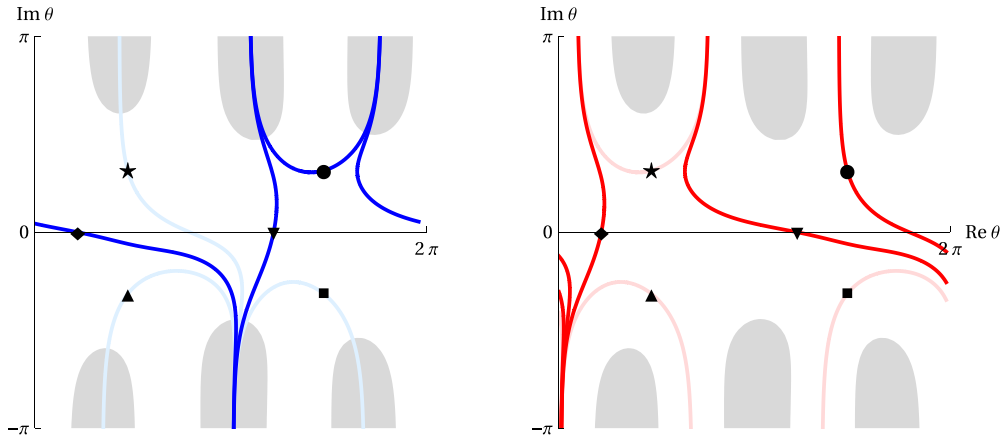
Figure 3. A demonstration of the rules of thimble homology. Both figures depict the complex-θ plane of action $\mathcal{S}$ featured in figure 1 with $\arg\beta = 0.4$. The black symbols lie on the stationary points of the action, and the grey regions depict the sets $\tilde{\Omega}_T$ of well-behaved regions at infinity (here $T = 5$). Left: lines show the thimbles of each stationary point. The thimbles necessary to recreate the cyclic path from left to right are darkly shaded, while those unnecessary for the task are lightly shaded. Notice that all thimbles come and go from the well-behaved regions. Right: lines show the antithimbles of each stationary point. Notice that those of the stationary points involved in the contour (shaded darkly) all intersect the desired contour (the real axis), while those not involved do not intersect it.

of thimbles! There is even a systematic way to determine the contribution from each thimble: for the stationary point $\sigma \in \Sigma$, let $\mathcal{K}_\sigma$ be its *antithimble*, defined by all points brought to s_σ by gradient *ascent* (and representing an element of the relative homology group $H_N(\tilde{\Omega}, \tilde{\Omega}_{-T})$). Then each thimble $\mathcal{J}_\sigma$ contributes to the contour with a weight given by its intersection pairing $n_\sigma = \langle \mathcal{C}, \mathcal{K}_\sigma \rangle$.

With these tools in hands, we can finally write the partition function as a sum over contributions from each thimble, or:

$$Z = \sum_{\sigma \in \Sigma} n_\sigma \oint_{\mathcal{J}_\sigma} ds\, e^{-\beta \mathcal{S}(s)}. \tag{4}$$

Under analytic continuation, the form of equation (4) generically persists. When the relative homology of the thimbles is unchanged by the continuation, the integer weights are likewise unchanged, and one can therefore use the knowledge of these weights in one regime to compute the partition function in the other. However, their relative homology can change, and when this happens the integer weights can be traded between stationary points. These trades occur when two thimbles intersect, or alternatively when one stationary point lies in the gradient descent of another. These places are called *Stokes points*, and the gradient descent trajectories that join two stationary points are called *Stokes lines*. An example of this behavior can be seen in figure 4.

The prevalence (or not) of Stokes points in a given continuation, and whether those that do appear affect the weights of stationary points of interest, is a concern for the analytic continuation of theories. If they do not occur or occur order-one times, one could reasonably hope to perform such a procedure. If they occur exponentially often in the system size, there is little hope of keeping track of the resulting weights, and analytic continuation is intractable.
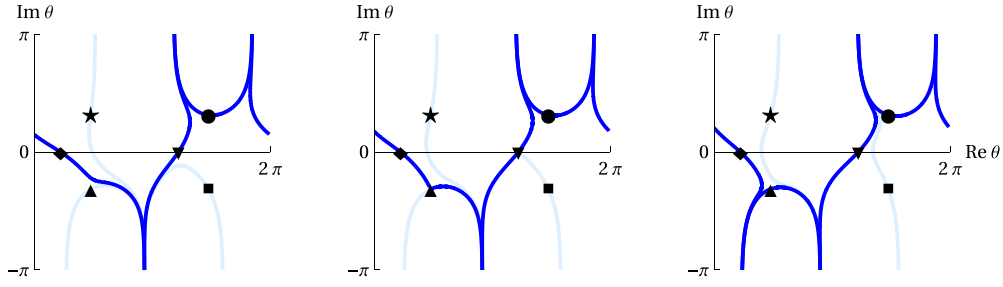
Figure 4. An example of a Stokes point in the continuation of the configuration space integral involving the action $\mathcal{S}$ featured in figure 1. Left: $\arg\beta = 1.176$. The collection of thimbles necessary to progress around from left to right, highlighted in a darker color, is the same as it was in figure 3. Center: $\arg\beta = 1.336$. The thimble $\mathcal{J}_\blacklozenge$ intersects the stationary point $\blacktriangle$ and its thimble, leading to a situation where the contour is not easily defined using thimbles. This is a Stokes point. Right: $\arg\beta = 1.496$. The Stokes point has passed, and the collection of thimbles necessary to produce the path has changed: now $\mathcal{J}_\blacktriangle$ must be included. Notice that in this figure, because of the symmetry of the pure models, the thimble $\mathcal{J}_\blacksquare$ also experiences a Stokes point, but this does not result in a change to the contour involving that thimble.

2.2. Gradient flow

The 'dynamics' describing thimbles is defined by gradient descent on the real part of the action, with a given thimble incorporating all trajectories which asymptotically flow to its associated stationary point. Since our configuration space is not necessary flat (as for the *spherical p*-spin models), we will have to do a bit of differential geometry to work out the form of the flow. Gradient descent on a complex manifold is given by:

$$\dot{s} = -\operatorname{grad}\operatorname{Re}\beta\mathcal{S} = -\left(\frac{\partial}{\partial s^*}\operatorname{Re}\beta\mathcal{S}\right)^{\sharp} = -\frac{\beta^*}{2}\frac{\partial\mathcal{S}^*}{\partial s^*}g^{-1}\frac{\partial}{\partial s}, \qquad (5)$$

where g is the metric and $\partial\mathcal{S}/\partial s^* = 0$ because the action is holomorphic. If the complex configuration space is $\mathbb{C}^N$ and the metric is diagonal, this means that the flow is proportional to the conjugate of the gradient, or $\dot{s} \propto -\beta^*(\partial\mathcal{S}/\partial s)^*$.

In the case we will consider here (namely, that of the spherical models), it will be more convenient to work in terms of coordinates in a flat embedding space than in terms of local coordinates in the curved space, e.g. in terms of $z \in \mathbb{C}^N$ instead of $s \in S^{N-1}$. Let $z : \tilde{\Omega} \to \mathbb{C}^N$ be an embedding of complex configuration space into complex euclidean space. The dynamics in the embedding space is given by:
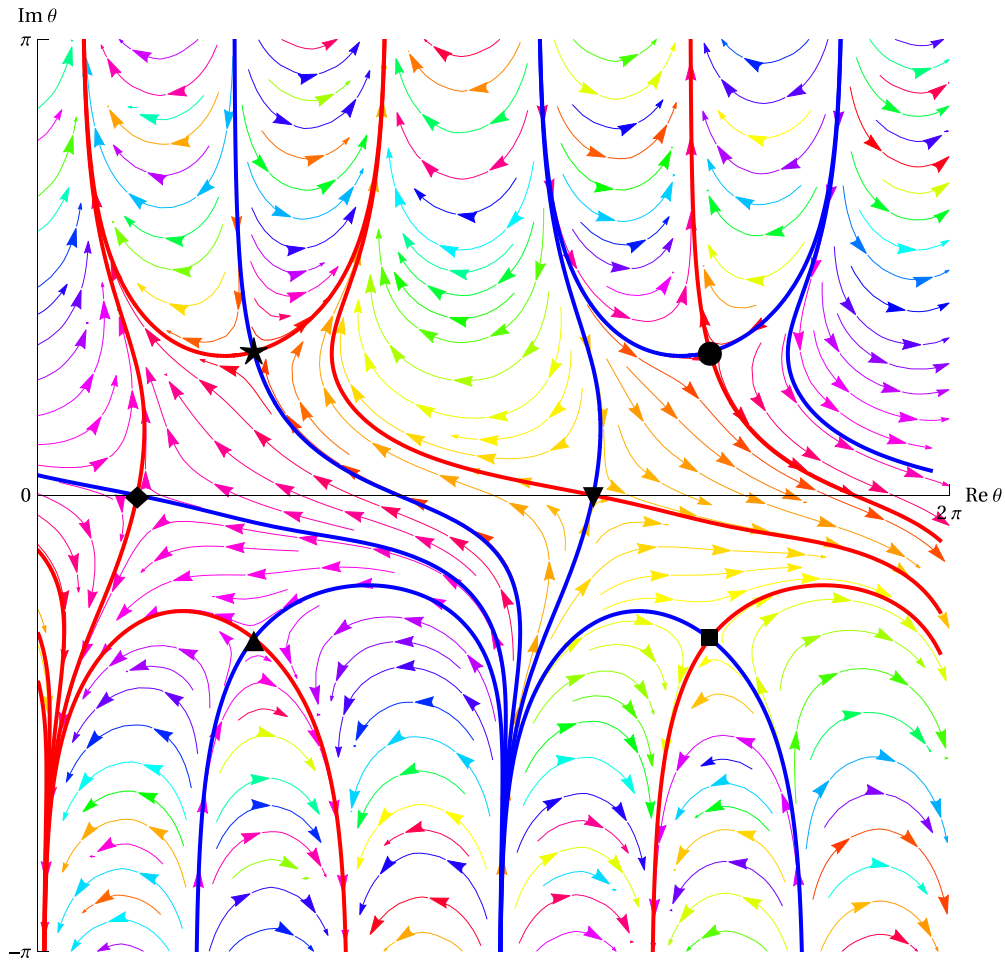
$$\dot{z} = -\frac{\beta^*}{2}\frac{\partial\mathcal{S}^*}{\partial z^*}(Dz)^*g^{-1}(Dz)^T\frac{\partial}{\partial z}, \qquad (6)$$

where $Dz = \partial z/\partial s$ is the Jacobian of the embedding. The embedding induces a metric on $\tilde{\Omega}$ by $g = (Dz)^\dagger Dz$. Writing $\partial = \partial/\partial z$, this gives:

$$\dot{z} = -\frac{\beta^*}{2}(\partial\mathcal{S})^\dagger(Dz)^*[(Dz)^\dagger(Dz)]^{-1}(Dz)^T = -\frac{1}{2}(\partial\mathcal{S})^\dagger P, \qquad (7)$$

which is nothing but the projection of $(\partial\mathcal{S})^*$ into the tangent space of the manifold, with the projection operator $P = (Dz)^*[(Dz)^\dagger(Dz)]^{-1}(Dz)^T$. Note that P is hermitian.

Figure 5. Example of gradient descent flow on the action $\mathcal{S}$ featured in figure 1 in the complex-θ plane, with $\arg\beta = 0.4$. Symbols denote the stationary points, while thick blue and red lines depict the thimbles and antithimbles, respectively. Streamlines of the flow equations are plotted in a color set by their value of $\operatorname{Im}\beta\mathcal{S}$; notice that the color is constant along each streamline.

Though the projection operator can be derived for any particular manifold by defining a coordinate system and computing it with the above definition, for simple manifolds like the sphere it can be guessed easily enough, as the unique hermitian operator that projects out the direction normal to the surface. For the sphere, this is:

$$P = I - \frac{zz^\dagger}{|z|^2}. \tag{8}$$

One can quickly verify that this operator indeed projects the dynamics onto the manifold: the vector perpendicular to the manifold at any point z is given by $\partial(z^T z) = z$, and $Pz = z - z|z|^2/|z|^2 = 0$. For any vector u perpendicular to z, i.e. $z^\dagger u = 0$, $Pu = u$, the identity. The flow field resulting from this dynamics for the 'circular' model is shown in figure 5.

Gradient descent on $\mathrm{Re}\,\beta\mathcal{S}$ is equivalent to Hamiltonian dynamics with the Hamiltonian $\mathrm{Im}\,\beta\mathcal{S}$ and conjugate coordinates given by the real and imaginary parts of each complex coordinate. This is because $(\tilde{\Omega}, g)$ is a Kähler manifold and therefore admits a symplectic structure, but it can be shown that the flow conserves the imaginary action using equation (7) and the holomorphic property of $\mathcal{S}$:

$$
\begin{aligned}
\frac{d}{dt}\mathrm{Im}\,\beta\mathcal{S} &= \dot{z}\partial\,\mathrm{Im}\,\beta\mathcal{S} + \dot{z}^*\partial^*\,\mathrm{Im}\,\beta\mathcal{S}\\
&= \frac{i}{4}\left((\beta\partial\mathcal{S})^\dagger P\beta\partial\mathcal{S} - (\beta\partial\mathcal{S})^T P^*(\beta\partial\mathcal{S})^*\right)\\
&= \frac{i|\beta|^2}{4}\left((\partial\mathcal{S})^\dagger P\partial\mathcal{S} - [(\partial\mathcal{S})^\dagger P\partial\mathcal{S}]^*\right)\\
&= \frac{i|\beta|^2}{4}\left(\|\partial\mathcal{S}\|^2 - (\|\partial\mathcal{S}\|^*)^2\right) = 0,
\end{aligned}
\tag{9}
$$

where $\|v\|^2 = v^\dagger P v$ is the norm of a complex vector v in the tangent space of the manifold. The flow of the action takes a simple form:

$$
\dot{\mathcal{S}} = \dot{z}\partial\mathcal{S} = -\frac{\beta^*}{2}(\partial\mathcal{S})^\dagger P\partial\mathcal{S} = -\frac{\beta^*}{2}\|\partial\mathcal{S}\|^2.
\tag{10}
$$

In the complex-$\mathcal{S}$ plane, dynamics is occurs along straight lines in a direction set by the argument of β.

2.3. The conditions for Stokes points

As we have seen, gradient descent on the real part of the action results in a flow that preserves the imaginary part of the action. Stokes lines, when they manifest, are topologically persistent so long as this conservation is respected: if a Stokes line connects two stationary points and the action is smoothly modified under the constraint that the imaginary parts of the two stationary points is held equal, the Stokes line will continue to connect them so long as the flow of a third stationary point does not sever their connection, i.e. so long as there is not a topological change in the flow. This implies that, despite being relatively low-dimensional surfaces of codimension N, thimble connections are found with a codimension one tuning of parameters, modulo the topological adjacency requirement. This means that, though not present in generic cases, Stokes points generically appear when a dimension-one curve is followed in parameter space.

Not all Stokes points result in the exchange of weight between thimbles. Examining figure 4 again, notice that the thimbles $\mathcal{J}_{\blacksquare}$ and $\mathcal{J}_{\blacktriangledown}$ also experience a Stokes point, but this does not result in a change to the contour involving those thimbles. This is because the integer weights can only be modified when a thimble that has some nonzero weight is downstream on the gradient descent flow, and therefore a necessary condition for a meaningful change in the thimble decomposition involving two stationary points σ and τ where $n_\sigma \neq 0$ and $n_\tau = 0$ is for $\mathrm{Re}\,\beta\mathcal{S}(s_\sigma) < \mathrm{Re}\,\beta\mathcal{S}(s_\tau)$.

Another necessary condition for the existence of a Stokes line between two stationary points is for those points to have the same imaginary action. However, this is not a sufficient condition. This can be seen in figure 6, which shows the thimbles of the circular 6-spin model. The argument of β has been chosen such that the stationary points marked by $\clubsuit$ and $\blacktriangle$ have exactly the same imaginary energy, and yet they do not share a thimble. This is because these stationary points are not adjacent: they are separated from each other by the thimbles of other
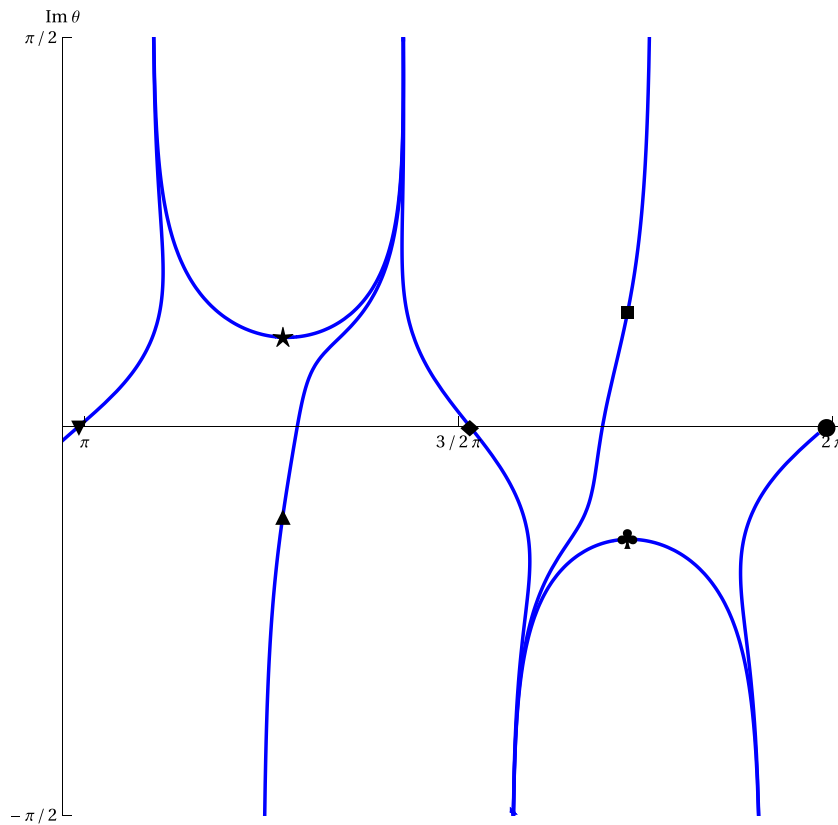
Figure 6. Some thimbles of the circular 6-spin model, where the argument of β has been chosen such that the imaginary parts of the action at the stationary points ♣ and ▲ are exactly the same (and, as a result of conjugation symmetry, the points ★ and ■).

stationary points. This is a consistent story in one complex dimension, since the codimension of the thimbles is one, and thimbles can divide space into regions. However, in higher dimensions thimbles do not have a codimension high enough to divide space into regions. Nonetheless, thimble intersections are still governed by a requirement for adjacency. Figure 7 shows a projection of the thimbles of an $N = 3$ 2-spin model, which is defined on the sphere. Because of an inversion symmetry of the model, stationary points on opposite sides of the sphere have identical energies, and therefore also share the same imaginary energy. However, their thimbles (blue and green in the figure) do not intersect. Here, they could not possibly intersect, since the real parts of their energy are also the same, and upward flow could therefore not connect them.

Determining whether stationary points are adjacent in this sense is a difficult problem, known as the global connection problem [3]. It is also difficult for us to reason rigorously about the properties of stationary point adjacency. However, we have a coarse argument for why, in generic cases with random actions, one should expect the typical number of adjacent stationary points to scale algebraically with dimension. First, notice that in order for two stationary points to be eligible to share a Stokes point, their thimbles must approach the same 'good' region of complex configuration space. This is because weight is traded at Stokes points when a facet of one thimble flops over another between good regions. Therefore, one can draw conclusions
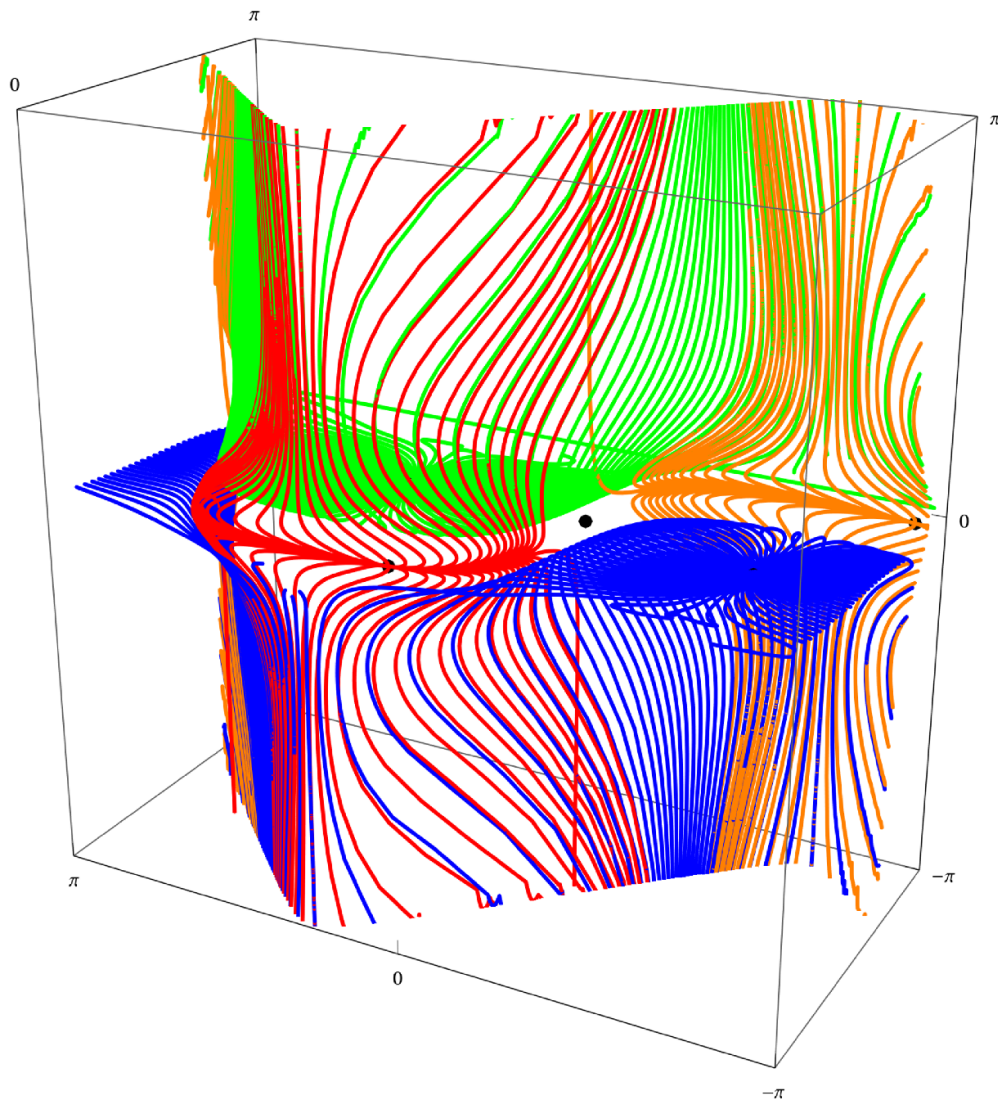
Figure 7. Thimbles of the $N = 3$ spherical 2-spin model projected into the $\mathrm{Re}\,\theta$, $\mathrm{Re}\,\phi$, $\mathrm{Im}\,\theta$ space. The blue and green lines trace gradient descent of the two minima, while the red and orange lines trace those of the two saddles. The location of the maxima are marked as points, but their thimbles are not shown.

about the number of stationary points eligible for a Stokes point with a given stationary point by examining the connectivity of the 'good' regions.

In the one-dimensional examples above, the 'good regions' for contours are zero-dimensional, making their topology discrete. However, in a D-dimensional case, these regions are $D - 1$ dimensional, and their topology is richer. Slices of thimbles evaluated at constant 'height' as measured by the real part of the action are topologically $D - 1$ spheres. These slices are known as the *vanishing cycles* of the thimble. At the extremal reaches of the configuration space manifold, these spherical slices form a mesh, sharing sections of their boundary with the slices of other thimbles and covering the extremal reaches like a net. Without some special
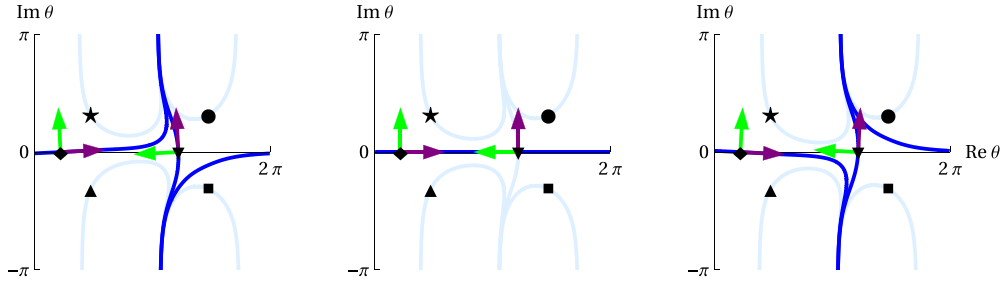
Figure 8. The behavior of thimble contours near $\arg\beta = 0$ for real actions. In all pictures, green arrows depict a canonical orientation of the thimbles relative to the real axis, while purple arrows show the direction of integration implied by the orientation. Left: $\arg\beta = -0.1$. To progress from left to right, one must follow the thimble from the minimum ◆ in the direction implied by its orientation, and then follow the thimble from the maximum ▼ *against* the direction implied by its orientation, from top to bottom. Therefore, $\mathcal{C} = \mathcal{J}_{\blacklozenge} - \mathcal{J}_{\blacktriangledown}$. Center: $\arg\beta = 0$. Here the thimble of the minimum covers almost all of the real axis, reducing the problem to the real configuration space integral. This is also a Stokes point. Right: $\arg\beta = 0.1$. Here, one follows the thimble of the minimum from left to right again, but now follows that of the maximum in the direction implied by its orientation, from bottom to top. Therefore, $\mathcal{C} = \mathcal{J}_{\blacklozenge} + \mathcal{J}_{\blacktriangledown}$.

symmetry to produce vertices in this mesh where many thimbles meet, such a mesh generally involves order D boundaries coming together in a given place. Considering the number of faces on a given extremal slice should also be roughly linear in D, one expects something like quadratic growth with D of eligible neighbors, something which gives a rough sense of locality in Stokes point interactions.

2.4. The structure of stationary points

The shape of each thimble in the vicinity of its stationary point can be described using an analysis of the hessian of the real part of the action at the stationary point. Here we will review some general properties of this hessian, which has rich structure because the action is holomorphic.

Writing down the hessian using the complex geometry of the previous section would be arduous. Luckily, we are only interested in the hessian at stationary points, and our manifolds of interest are constraint surfaces. These two facts allow us to find the hessian at stationary points using a simpler technique, that of Lagrange multipliers.

Suppose that our complex manifold $\tilde{\Omega}$ is defined by all points $z \in \mathbb{C}^N$ such that $g(z) = 0$ for some holomorphic function g. In the case of the spherical models, $g(z) = \frac{1}{2}(z^T z - N)$. Introducing the Lagrange multiplier μ, we define the constrained action:

$$\tilde{\mathcal{S}}(z) = \mathcal{S}(z) - \mu g(z). \tag{11}$$

The condition for a stationary point is that $\partial\tilde{\mathcal{S}} = 0$. This implies that, at any stationary point, $\partial\mathcal{S} = \mu\partial g$. In particular, if $\partial g^T \partial g \neq 0$, we find the value for the Lagrange multiplier μ as:

$$\mu = \frac{\partial g^T \partial \mathcal{S}}{\partial g^T \partial g}. \tag{12}$$

As a condition for a stationary point, this can be intuited as projecting out the normal to the constraint surface ∂g from the gradient of the unconstrained action. It implies that the hessian with respect to the complex embedding coordinate z at any stationary point is:

$$\text{Hess}\,\mathcal{S} = \partial\partial\tilde{\mathcal{S}} = \partial\partial\mathcal{S} - \frac{\partial g^T \partial \mathcal{S}}{\partial g^T \partial g}\partial\partial g. \tag{13}$$

In practice one must neglect the directions normal to the constraint surface by projecting them out using P from the previous section, i.e. $P\,\text{Hess}\,\mathcal{S}P^T$. For notational simplicity we will not include this here.

In order to describe the structure of thimbles, one must study the hessian of $\text{Re}\,\beta\mathcal{S}$, since it is the upward directions in the flow on the real action in the vicinity of stationary points which define them. We first pose the problem as one of $2N$ real variables $x, y \in \mathbb{R}^N$ with $z = x + iy$. The hessian of the real part of the action with respect to these real variables is:

$$\text{Hess}_{x,y}\,\text{Re}\,\beta\mathcal{S} = \begin{bmatrix} \partial_x\partial_x\,\text{Re}\,\beta\tilde{\mathcal{S}} & \partial_y\partial_x\,\text{Re}\,\beta\tilde{\mathcal{S}} \\ \partial_x\partial_y\,\text{Re}\,\beta\tilde{\mathcal{S}} & \partial_y\partial_y\,\text{Re}\,\beta\tilde{\mathcal{S}} \end{bmatrix}. \tag{14}$$

This can be simplified using the fact that the action is holomorphic, which means that it obeys the Cauchy–Riemann equations:

$$\partial_x\,\text{Re}\,\tilde{\mathcal{S}} = \partial_y\,\text{Im}\,\tilde{\mathcal{S}} \qquad \partial_y\,\text{Re}\,\tilde{\mathcal{S}} = -\partial_x\,\text{Im}\,\tilde{\mathcal{S}}. \tag{15}$$

Using these relationships alongside the Wirtinger derivative $\partial \equiv \frac{1}{2}(\partial_x - i\partial_y)$ allows the order of the derivatives and the real or imaginary parts to be commuted, with:

$$\begin{aligned} \partial_x\,\text{Re}\,\tilde{\mathcal{S}} = \text{Re}\,\partial\tilde{\mathcal{S}} \qquad \partial_y\,\text{Re}\,\tilde{\mathcal{S}} = -\text{Im}\,\partial\tilde{\mathcal{S}} \\ \partial_x\,\text{Im}\,\tilde{\mathcal{S}} = \text{Im}\,\partial\tilde{\mathcal{S}} \qquad \partial_y\,\text{Im}\,\tilde{\mathcal{S}} = \text{Re}\,\partial\tilde{\mathcal{S}} \end{aligned}. \tag{16}$$

Using these relationships, the hessian equation (14) can be written in the more manifestly complex way:

$$\begin{aligned} \text{Hess}_{x,y}\,\text{Re}\,\beta\mathcal{S} &= \begin{bmatrix} \text{Re}\,\beta\partial\partial\tilde{\mathcal{S}} & -\text{Im}\,\beta\partial\partial\tilde{\mathcal{S}} \\ -\text{Im}\,\beta\partial\partial\tilde{\mathcal{S}} & -\text{Re}\,\beta\partial\partial\tilde{\mathcal{S}} \end{bmatrix} \\ &= \begin{bmatrix} \text{Re}\,\beta\,\text{Hess}\,\mathcal{S} & -\text{Im}\,\beta\,\text{Hess}\,\mathcal{S} \\ -\text{Im}\,\beta\,\text{Hess}\,\mathcal{S} & -\text{Re}\,\beta\,\text{Hess}\,\mathcal{S} \end{bmatrix}, \end{aligned} \tag{17}$$

where $\text{Hess}\,\mathcal{S}$ is the hessian with respect to z given in (13).

The eigenvalues and eigenvectors of the hessian are important for evaluating thimble integrals, because those associated with upward directions provide a local basis for the surface of the thimble. Suppose that $v_x, v_y \in \mathbb{R}^N$ are such that:

$$(\text{Hess}_{x,y}\,\text{Re}\,\beta\mathcal{S})\begin{bmatrix} v_x \\ v_y \end{bmatrix} = \lambda\begin{bmatrix} v_x \\ v_y \end{bmatrix}, \tag{18}$$

where the eigenvalue λ must be real because the hessian is real symmetric. The problem can be put into a more obviously complex form by a change of basis. Writing $v = v_x + iv_y$, we find:

$$\begin{aligned} &\begin{bmatrix} 0 & (i\beta\,\text{Hess}\,\mathcal{S})^* \\ i\beta\,\text{Hess}\,\mathcal{S} & 0 \end{bmatrix}\begin{bmatrix} v \\ iv^* \end{bmatrix} \\ &= \begin{bmatrix} 1 & i \\ i & 1 \end{bmatrix}(\text{Hess}_{x,y}\,\text{Re}\,\beta\mathcal{S})\begin{bmatrix} 1 & i \\ i & 1 \end{bmatrix}^{-1}\begin{bmatrix} 1 & i \\ i & 1 \end{bmatrix}\begin{bmatrix} v_x \\ v_y \end{bmatrix} \\ &= \lambda\begin{bmatrix} 1 & i \\ i & 1 \end{bmatrix}\begin{bmatrix} v_x \\ v_y \end{bmatrix} = \lambda\begin{bmatrix} v \\ iv^* \end{bmatrix}. \end{aligned} \tag{19}$$

It therefore follows that the eigenvalues and vectors of the real hessian satisfy the equation:

$$\beta \operatorname{Hess} \mathcal{S} v = \lambda v^*, \tag{20}$$

a sort of generalized eigenvalue problem whose solutions are called the *Takagi vectors* of $\operatorname{Hess}\mathcal{S}$ [4]. If we did not know the eigenvalues were real, we could still see it from the second implied equation, $(\beta \operatorname{Hess}\mathcal{S})^* v^* = \lambda v$, which is the conjugate of the first if $\lambda^* = \lambda$.

Something hidden in the structure of the real hessian but more clear in its complex form is that each eigenvalue comes in a pair, since:

$$\beta \operatorname{Hess} \mathcal{S}(iv) = i\lambda v^* = -\lambda(iv). \tag{21}$$

Therefore, if λ satisfies (20) with Takagi vector v, than so does $-\lambda$ with associated Takagi vector iv, rotated in the complex plane. It follows that each stationary point has an equal number of descending and ascending directions, i.e. the index of each stationary point is N. For a stationary point in a real problem this might seem strange, because there are clear differences between minima, maxima, and saddles of different index. However, for such a stationary point, its N real Takagi vectors that determine its index in the real problem are accompanied by N purely imaginary Takagi vectors, pointing into the complex plane and each with the negative eigenvalue of its partner. A real minimum on the real manifold therefore has N downward directions alongside its N upward ones, all pointing directly into complex configuration space.

The effect of changing the argument of β is revealed by (20). Writing $\beta = |\beta|e^{i\phi}$ and dividing both sides by $|\beta|e^{i\phi/2}$, one finds:

$$\operatorname{Hess}\mathcal{S}(e^{i\phi/2}v) = \frac{\lambda}{|\beta|} e^{-i\phi/2} v^* = \frac{\lambda}{|\beta|}(e^{i\phi/2}v)^*. \tag{22}$$

Therefore, one only needs to consider solutions to the Takagi problem for the action alone, $\operatorname{Hess}\mathcal{S}v_0 = \lambda_0 v_0^*$, and then rotate the resulting Takagi vectors by a constant phase corresponding to half the argument of β, or $v(\phi) = v_0 e^{-i\phi/2}$. One can see this in the examples of figures 4 and 8, where increasing the argument of β from left to right produces a clockwise rotation of the thimbles in the complex-θ plane.

The eigenvalues associated with the Takagi vectors can be further related to properties of the complex symmetric matrix $\beta \operatorname{Hess}\mathcal{S}$. Suppose that $u \in \mathbb{R}^N$ satisfies the eigenvalue equation:

$$(\beta \operatorname{Hess}\mathcal{S})^\dagger (\beta \operatorname{Hess}\mathcal{S})u = \sigma u, \tag{23}$$

for some positive real σ (because $(\beta \operatorname{Hess}S)^\dagger (\beta \operatorname{Hess}\mathcal{S})$ is self-adjoint and positive definite). The square root of these numbers, $\sqrt{\sigma}$, are the definition of the *singular values* of $\beta \operatorname{Hess}\mathcal{S}$. A direct relationship between these singular values and the eigenvalues of the real hessian immediately follows by taking a Takagi vector $v \in \mathbb{C}$ that satisfies equation (20), and writing:

$$\begin{aligned}
\sigma v^\dagger u &= v^\dagger (\beta \operatorname{Hess}\mathcal{S})^\dagger (\beta \operatorname{Hess}\mathcal{S})u = (\beta \operatorname{Hess}\mathcal{S}v)^\dagger (\beta \operatorname{Hess}\mathcal{S})u \\
&= (\lambda v^*)^\dagger (\beta \operatorname{Hess}\mathcal{S})u = \lambda v^T (\beta \operatorname{Hess}\mathcal{S})u = \lambda^2 v^\dagger u.
\end{aligned} \tag{24}$$

Thus if $v^\dagger u \neq 0$, $\lambda^2 = \sigma$. It follows that the eigenvalues of the real hessian are the singular values of the complex matrix $\beta \operatorname{Hess}\mathcal{S}$, and the Takagi vectors coincide with the eigenvectors of the singular value problem up to a complex factor.

2.5. Evaluating thimble integrals

After all the work of decomposing an integral into a sum over thimbles, one eventually wants to evaluate it. For large $|\beta|$ and in the absence of any Stokes points, one can come to a nice asymptotic expression. For a thorough account of evaluating these integrals (including *at* Stokes points), see Howls [3].

Suppose that $\sigma \in \Sigma$ is a stationary point at $s_\sigma \in \tilde{\Omega}$ with a thimble $\mathcal{J}_\sigma$ that is not involved in any upstream Stokes points. Define its contribution to the partition function (neglecting the integer weight) as:

$$Z_\sigma = \oint_{\mathcal{J}_\sigma} ds\, e^{-\beta \mathcal{S}(s)}. \tag{25}$$

To evaluate this contour integral in the limit of large $|\beta|$, we will make use of the saddle point method, since the integral will be dominated by its value at and around the stationary point, where the real part of the action is by construction at its minimum on the thimble and the integrand is therefore largest.

We will make a change of coordinates $u(s) : \mathcal{J}_\sigma \to \mathbb{R}^D$, where D is the dimension of the manifold ($D = N - 1$ for the spherical models), such that:

$$\beta \mathcal{S}(s) = \beta \mathcal{S}(s_\sigma) + \frac{|\beta|}{2} u(s)^T u(s), \tag{26}$$

and the direction of each $\partial u / \partial s$ is aligned with the direction of the contour. This is possible because, in the absence of any Stokes points, the eigenvectors of the hessian at the stationary point associated with positive eigenvalues provide a basis for the thimble. The coordinates u can be real because the imaginary part of the action is constant on the thimble, and therefore stays with the value it holds at the stationary point, and the real part is at its minimum. The preimage of $u(s)^T u(s)$ gives the vanishing cycles of the thimble, discussed in an earlier subsection.

The coordinates u can be constructed implicitly in the close vicinity of the stationary point, with their inverse being:

$$s(u) = s_\sigma + \sum_{i=1}^{D} \sqrt{\frac{|\beta|}{\lambda^{(i)}}} v^{(i)} u_i + O(u^2), \tag{27}$$

where the sum is over pairs (λ, v) which satisfy (20) and have $\lambda > 0$. It is straightforward to confirm that these coordinates satisfy (26) asymptotically close to the stationary point, as:

$$
\begin{aligned}
\beta \mathcal{S}(s(u)) &= \beta \mathcal{S}(s_\sigma) + \frac{1}{2}(s(u) - s_\sigma)^T (\beta \operatorname{Hess} \mathcal{S})(s(u) - s_\sigma) + \cdots \\
&= \beta \mathcal{S}(s_\sigma) + \frac{|\beta|}{2} \sum_{ij} \frac{v_k^{(i)}}{\sqrt{\lambda^{(i)}}} (\beta[\operatorname{Hess}\mathcal{S}]_{k\ell}) \frac{v_\ell^{(j)}}{\sqrt{\lambda^{(j)}}} u_i u_j + \cdots \\
&= \beta \mathcal{S}(s_\sigma) + \frac{|\beta|}{2} \sum_{ij} \frac{v_k^{(i)}}{\sqrt{\lambda^{(i)}}} \frac{\lambda^{(j)} \left(v_k^{(j)}\right)^*}{\sqrt{\lambda^{(j)}}} u_i u_j + \cdots \\
&= \beta \mathcal{S}(s_\sigma) + \frac{|\beta|}{2} \sum_{ij} \frac{\sqrt{\lambda^{(j)}}}{\sqrt{\lambda^{(i)}}} \delta_{ij} u_i u_j + \cdots \\
&= \beta \mathcal{S}(s_\sigma) + \frac{|\beta|}{2} \sum_i u_i^2 + \cdots
\end{aligned}
\tag{28}
$$

The Jacobian of this transformation is:

$$\frac{\partial s_i}{\partial u_j} = \sqrt{\frac{|\beta|}{\lambda^{(j)}}} v_i^{(j)} + \cdots = \sqrt{\frac{1}{\lambda_0^{(j)}}} v_i^{(j)} + \cdots, \tag{29}$$

where $\lambda_0^{(j)} = \lambda^{(j)}/|\beta|$ is the jth eigenvalue of the hessian evaluated at the stationary point for $\beta = 1$. This is naïvely an $N \times D$ matrix, because the Takagi vectors are N dimensional, but care must be taken to project each into the tangent space of the manifold to produce a $D \times D$ matrix. This lets us write $U_{ij} = v_i^{(j)}$ a $D \times D$ unitary matrix, whose determinant will give the correct phase for the measure.

We therefore have:

$$Z_\sigma = e^{-\beta\mathcal{S}(s_\sigma)} \int du \det \frac{ds}{du} e^{-\frac{|\beta|}{2} u^T u}, \tag{30}$$

which is exact. Now we take the saddle point approximation, assuming the integral is dominated by its value at the stationary point, and therefore that the determinant can be approximated by its value at the stationary point. This gives:

$$\begin{aligned} Z_\sigma &\simeq e^{-\beta\mathcal{S}(s_\sigma)} \det \frac{ds}{du}\bigg|_{s=s_\sigma} \int du\, e^{-\frac{|\beta|}{2} u^T u} \\ &= e^{-\beta\mathcal{S}(s_\sigma)} \left(\prod_i^D \sqrt{\frac{1}{\lambda_0^{(i)}}} \right) \det U \left(\frac{2\pi}{|\beta|} \right)^{D/2} \\ &= e^{-\beta\mathcal{S}(s_\sigma)} |\det \mathrm{Hess}\,\mathcal{S}(s_\sigma)|^{-1/2} \det U \left(\frac{2\pi}{|\beta|} \right)^{D/2}. \end{aligned} \tag{31}$$

We are left with evaluating the determinant of the unitary part of the coordinate transformation. In circumstances you may be used to, only the absolute value of the determinant from the coordinate transformation is relevant, and since the determinant of a unitary matrix is always magnitude one, it does not enter the computation. However, because we are dealing with a contour integral, the directions matter, and there is not an absolute value around the determinant. Therefore, we must determine the phase that it contributes.

This is difficult in general, but for real stationary points it can be reasoned out easily. Take the convention that direction of contours along the real line is with the standard orientation. Then, when $\beta = 1$ a stationary point of index k has $D - k$ real Takagi vectors and k purely imaginary Takagi vectors that correspond with upward directions in the flow and contribute to its thimble. The matrix of Takagi vectors can therefore be written $U = i^k O$ for an orthogonal matrix O, and with all eigenvectors canonically oriented $\det O = 1$. We therefore have $\det U = i^k$ when $\beta = 1$. As the argument of β is changed, we know how the eigenvectors change: by a factor of $e^{-i\phi/2}$ for $\phi = \arg \beta$. Therefore, the contribution for general β is $\det U = (e^{-i\phi/2})^D i^k$. We therefore have, for real stationary points of a real action,

$$\begin{aligned} Z_\sigma &\simeq \left(\frac{2\pi}{|\beta|} \right)^{D/2} e^{-i\phi D/2} i^{k_\sigma} |\det \mathrm{Hess}\,\mathcal{S}(s_\sigma)|^{-\frac{1}{2}} e^{-\beta\mathcal{S}(s_\sigma)} \\ &= \left(\frac{2\pi}{\beta} \right)^{D/2} i^{k_\sigma} |\det \mathrm{Hess}\,\mathcal{S}(s_\sigma)|^{-\frac{1}{2}} e^{-\beta\mathcal{S}(s_\sigma)}. \end{aligned} \tag{32}$$

We can see that the large-β approximation is consistent with the relationship between thimble orientation and integer weight outlined in figure 8. There, it is seen that taking the argument of β through zero results in a series of Stokes points among real stationary points

of a real action which switches the sign of the integer weights of thimbles with odd index and preserves the integer weights of thimbles with even index. For a real action, taking $\beta \to \beta^*$ should simply take $Z \to Z^*$. Using the formula above, we find:

$$Z(\beta)^* = \sum_{\sigma \in \Sigma_0} n_\sigma Z_\sigma(\beta)^* = \sum_{\sigma \in \Sigma_0} n_\sigma (-1)^{k_\sigma} Z_\sigma(\beta^*) = Z(\beta^*), \tag{33}$$

as expected.

3. The ensemble of symmetric complex-normal matrices

Having introduced the general method for analytic continuation, we will now begin dealing with the implications of actions defined in many dimensions with disorder. We saw in section 2.4 that the singular values of the complex hessian of the action at each stationary point are important to the study of thimbles. Hessians are symmetric matrices by construction. For real actions of real variables, the study of random symmetric matrices with Gaussian entries provides insight into a wide variety of problems. In our case, we will find the relevant ensemble is that of random symmetric matrices with *complex-normal* entries. In this section, we will introduce this distribution, review its known properties, and derive its singular value distribution in the large-matrix limit.

The complex normal distribution with zero mean is the unique Gaussian distribution in one complex variable Z whose variances are $\overline{Z^*Z} = \overline{|Z|^2} = \Gamma$ and $\overline{Z^2} = C$. Γ is positive, and $|C| \leqslant \Gamma$. The special case of $C = \Gamma$, where the variance of the complex variable and its covariance with its conjugate are the same, reduces to the ordinary normal distribution. The case where $C = 0$ results in the real and imaginary parts of Z being uncorrelated, in what is known as the standard complex normal distribution. The probability density function for general Γ and C is defined by:

$$p(z \mid \Gamma, C) = \frac{1}{\pi\sqrt{\Gamma^2 - |C|^2}} \exp\left\{\frac{1}{2} \begin{bmatrix} z^* & z \end{bmatrix} \begin{bmatrix} \Gamma & C \\ C^* & \Gamma \end{bmatrix}^{-1} \begin{bmatrix} z \\ z^* \end{bmatrix}\right\}. \tag{34}$$

This is the same as writing $Z = X + iY$ and requiring that the mutual distribution in X and Y be normal with $\overline{X^2} = \Gamma + \operatorname{Re}C$, $\overline{Y^2} = \Gamma - \operatorname{Re}C$, and $\overline{XY} = \operatorname{Im}C$.

We will consider an ensemble of random $N \times N$ matrices $B = A + \lambda_0 I$, where the entries of A are complex-normal distributed with variances $\overline{|A_{ij}|^2} = \Gamma_0/N$ and $\overline{A_{ij}^2} = C_0/N$, and λ_0 is a constant shift to the diagonal. The eigenvalue distribution of the matrices A is already known to take the form of an elliptical ensemble in the large-N limit, with constant support inside the ellipse defined by:

$$\left(\frac{\operatorname{Re}(\lambda e^{i\theta})}{1 + |C_0|/\Gamma_0}\right)^2 + \left(\frac{\operatorname{Im}(\lambda e^{i\theta})}{1 - |C_0|/\Gamma_0}\right)^2 < \Gamma_0, \tag{35}$$

where $\theta = \frac{1}{2}\arg C_0$ [5]. The eigenvalue spectrum of B is therefore constant inside the same ellipse translated so that its center lies at λ_0. Examples of these distributions are shown in the insets of figure 9.

When $C = 0$ and the elements of A are standard complex normal, the singular value distribution of B is a complex Wishart distribution. For $C \neq 0$ the problem changes, and to our knowledge a closed form of the singular value distribution is not in the literature. We have

worked out an implicit form for the singular value spectrum using the replica method, first published in [6].

The singular values of B correspond with the square-root of the eigenvalues of $B^\dagger B$, but also they correspond to the absolute value of the eigenvalues of the real $2N \times 2N$ block matrix:

$$\begin{bmatrix} \operatorname{Re} B & -\operatorname{Im} B \\ -\operatorname{Im} B & -\operatorname{Re} B \end{bmatrix}, \tag{36}$$

as we saw in section 2.4. The $2N \times 2N$ problem is easier to treat analytically than the $N \times N$ one because the matrix under study is linear in the entries of B. The eigenvalue spectrum of this block matrix can be studied by ordinary techniques from random matrix theory. Defining the 'partition function':

$$Z(\sigma) = \int dx\, dy \exp \left\{ -\frac{1}{2} \begin{bmatrix} x & y \end{bmatrix} \left(\sigma I - \begin{bmatrix} \operatorname{Re} B & -\operatorname{Im} B \\ -\operatorname{Im} B & -\operatorname{Re} B \end{bmatrix} \right) \begin{bmatrix} x \\ y \end{bmatrix} \right\}, \tag{37}$$

implies a Green function:

$$G(\sigma) = \frac{\partial}{\partial \sigma} \log Z(\sigma), \tag{38}$$

whose poles give the singular values of B. This can be put into a manifestly complex form using the method of section 2.4, with the same linear transformation of $x, y \in \mathbb{R}^N$ into $z \in \mathbb{C}^N$. This gives:

$$\begin{aligned} Z(\sigma) &= \int dz^* dz \exp \left\{ -\frac{1}{2} \begin{bmatrix} z^* & -iz \end{bmatrix} \left(\sigma I - \begin{bmatrix} 0 & (iB)^* \\ iB & 0 \end{bmatrix} \right) \begin{bmatrix} z \\ iz^* \end{bmatrix} \right\} \\ &= \int dz^* dz \exp \left\{ -\frac{1}{2} \left(2z^\dagger z \sigma - z^\dagger B^* z^* - z^T B z \right) \right\} \\ &= \int dz^* dz \exp \left\{ -z^\dagger z \sigma + \operatorname{Re} (z^T B z) \right\} \end{aligned} \tag{39}$$

which is a general expression for the singular values σ of a symmetric complex matrix B.

Introducing replicas to eliminate the logarithm in the Green function [7] gives:

$$G(\sigma) = \lim_{n \to 0} \int dz^* dz\, z_0^\dagger z_0 \exp \left\{ -\sum_{\alpha}^{n} \left[z_\alpha^\dagger z_\alpha \sigma + \operatorname{Re} \left(z_\alpha^T B z_\alpha \right) \right] \right\} \tag{40}$$

The average is then made over the entries of B and Hubbard–Stratonovich is used to change variables to the replica matrices $N\alpha_{\alpha\beta} = z_\alpha^\dagger z_\beta$ and $N\chi_{\alpha\beta} = z_\alpha^T z_\beta$, and a series of replica vectors. The replica-symmetric ansatz leaves all replica vectors zero, and $\alpha_{\alpha\beta} = \alpha_0 \delta_{\alpha\beta}$, $\chi_{\alpha\beta} = \chi_0 \delta_{\alpha\beta}$. The result is:

$$\begin{aligned} \overline{G}(\sigma) = N \lim_{n \to 0} \int d\alpha_0\, d\chi_0^*\, d\chi_0 \alpha_0 \exp \Big\{ & nN \Big[1 + \frac{1}{8}\Gamma_0 \alpha_0^2 - \frac{\alpha_0 \sigma}{2} \\ & + \frac{1}{2} \log(\alpha_0^2 - |\chi_0|^2) + \frac{1}{2} \operatorname{Re} \left(\frac{1}{4} C_0^* \chi_0^2 + \lambda_0^* \chi_0 \right) \Big] \Big\}. \end{aligned} \tag{41}$$

The argument of the exponential has several saddles. The solutions α_0 are the roots of a sixth-order polynomial, and the root with the smallest value of $\operatorname{Re} \alpha_0$ gives the correct solution in all the cases we studied. A detailed analysis of the saddle point integration is needed to
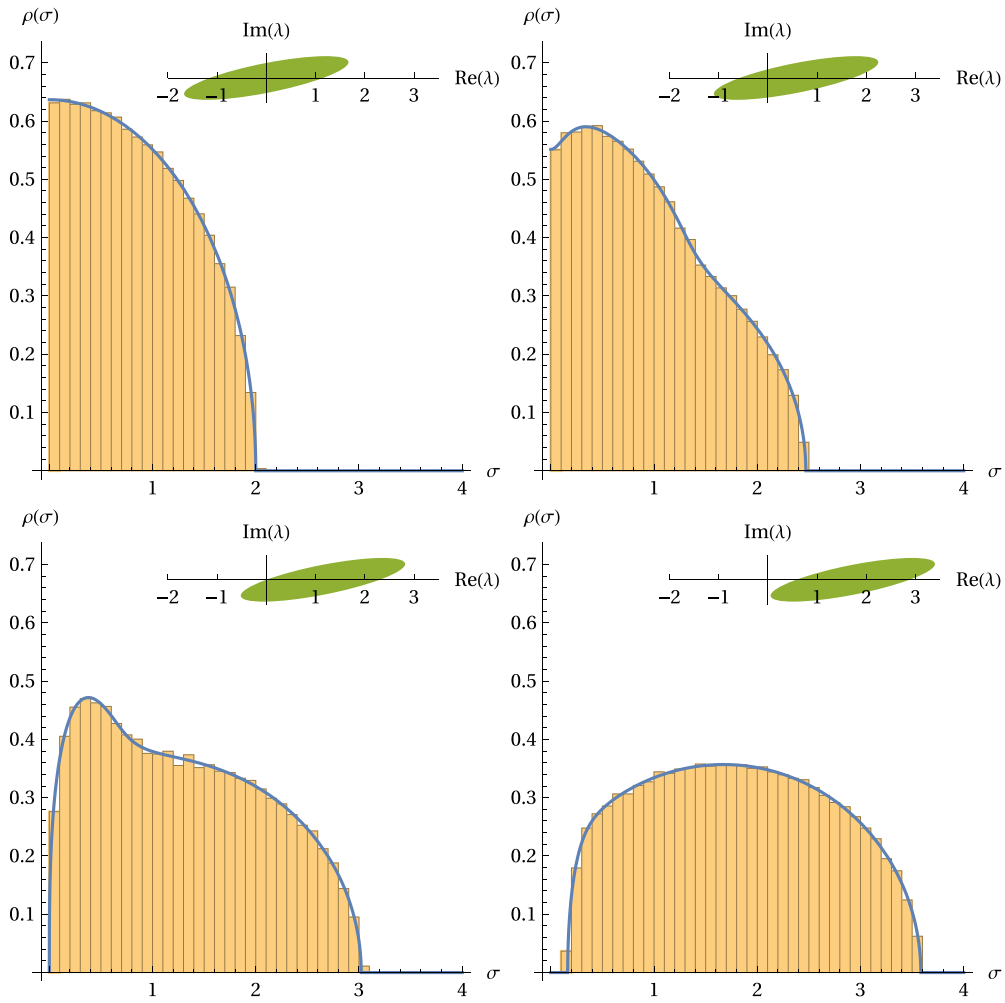
Figure 9. Eigenvalue and singular value spectra of a random matrix $B = A + \lambda_0 I$, where the entries of A are complex-normal distributed with $N\overline{|A_{ij}|^2} = \Gamma_0 = 1$ and $N\overline{A_{ij}^2} = C_0 = \frac{7}{10}e^{i\pi/8}$. The diagonal shifts differ in each plot, with (a) $\lambda_0 = 0$, (b) $\lambda_0 = \frac{1}{2}|\lambda_{\text{gap}}|$, (c) $\lambda_0 = |\lambda_{\text{gap}}|$, and (d) $\lambda_0 = \frac{3}{2}|\lambda_{\text{gap}}|$. The shaded region of each inset shows the support of the eigenvalue distribution (35). The solid line on each plot shows the distribution of singular values (42), while the overlaid histogram shows the empirical distribution from $2^{10} \times 2^{10}$ complex normal matrices.

understand why this is so. Evaluated at such a solution, the density of singular values follows from the jump across the cut in the infinite-N limit, or:

$$\rho(\sigma) = \frac{1}{i\pi N}\left(\lim_{\text{Im}\,\sigma \to 0^+} \overline{G}(\sigma) - \lim_{\text{Im}\,\sigma \to 0^-} \overline{G}(\sigma)\right). \tag{42}$$

Examples of this distribution can be seen in figure 9 compared with numeric experiments.

The formation of a gap in the singular value spectrum naturally corresponds to the origin leaving the support of the eigenvalue spectrum. Weyl's theorem requires that the product over

the norm of all eigenvalues must not be greater than the product over all singular values [8]. Therefore, the absence of zero eigenvalues implies the absence of zero singular values. The determination of the constant shift λ_0 at which the distribution of singular values becomes gapped is reduced to the geometry problem of determining when the boundary of the ellipse defined in (35) intersects the origin, and yields:

$$|\lambda_{\text{gap}}|^2 = \Gamma_0 \frac{(1 - |\delta|^2)^2}{1 + |\delta|^2 - 2|\delta|\cos(\arg\delta + 2\arg\lambda_0)}, \tag{43}$$

for $\delta = C_0/\Gamma_0$. Because the support is an ellipse, this naturally depends on the argument of λ_0, or the direction in the complex plane in which the distribution is shifted.

4. The *p*-spin spherical models

The p-spin spherical models are defined by the action:

$$\mathcal{S}(x) = \sum_{p=2}^{\infty} a_p \mathcal{S}_p(x), \tag{44}$$

which is a sum of the 'pure' p-spin actions:

$$\mathcal{S}_p(x) = \frac{1}{p!} \sum_{i_1 \cdots i_p} J_{i_1 \cdots i_p} x_{i_1} \cdots x_{i_p}. \tag{45}$$

The variables $x \in \mathbb{R}^N$ are constrained to lie on the sphere $x^2 = N$, making the model $D = N - 1$ dimensional. The couplings J form totally symmetric p-tensors whose components are normally distributed with zero mean and variance $\overline{J^2} = p!/2N^{p-1}$. The 'pure' p-spin models have $a_i = \delta_{ip}$, while the mixed have some more complicated set of coefficients a.

The configuration space manifold $\Omega = \{x \mid x^2 = N, x \in \mathbb{R}^N\}$ has a complex extension $\tilde{\Omega} = \{z \mid z^2 = N, z \in \mathbb{C}^N\}$. The natural extension of the Hamiltonian equation (44) to this complex manifold by replacing x with $z \in \mathbb{C}^N$ is holomorphic. The normal to this manifold at any point $z \in \tilde{\Omega}$ is always in the direction z. The projection operator onto the tangent space of this manifold is given by:

$$P = I - \frac{zz^\dagger}{|z|^2}, \tag{46}$$

where indeed $Pz = z - z|z|^2/|z|^2 = 0$ and $Pz' = z'$ for any z' orthogonal to z. When studying stationary points, the constraint can be added to the action using a Lagrange multiplier μ by writing:

$$\tilde{\mathcal{S}}(z) = \mathcal{S}(z) - \frac{\mu}{2}(z^T z - N). \tag{47}$$

The gradient of the constraint is simple with $\partial g = z$, and (12) implies that:

$$\mu = \frac{1}{N} z^T \partial \mathcal{S} = \sum_{p=2}^{\infty} a_p p \frac{\mathcal{S}_p(z)}{N}. \tag{48}$$

For the pure p-spin in particular this implies that $\mu = p\epsilon$ for specific energy $\epsilon = \mathcal{S}_p/N$.

4.1. 2-spin

The pure 2-spin model is diagonalizable and therefore exactly solvable, and is not complex in the sense of having a superextensive number of stationary points in its action. However, it makes a good exercise of how the ideas of analytic continuation will apply in the literally more complex case of the p-spin for $p > 2$. The Hamiltonian of the pure 2-spin model is defined by:

$$\mathcal{S}_2(z) = \frac{1}{2}z^T J z, \tag{49}$$

where the matrix J is generically diagonalizable. In a diagonal basis, $J_{ij} = \lambda_i \delta_{ij}$. Then $\partial_i H = \lambda_i z_i$. We will henceforth assume to be working in this basis. The constrained action is:

$$\tilde{\mathcal{S}}(z) = \mathcal{S}_2(z) - \epsilon(z^T z - N), \tag{50}$$

Stationary points must satisfy:

$$0 = \partial_i \tilde{\mathcal{S}} = (\lambda_i - 2\epsilon)z_i, \tag{51}$$

which is only possible for $z_i = 0$ or $\epsilon = \frac{1}{2}\lambda_i$. Generically the λ_i will all differ, so this can only be satisfied for one λ_i at a time, and to be a stationary point all other z_j must be zero. In the direction in question,

$$\frac{1}{N}\frac{1}{2}\lambda_i z_i^2 = \epsilon = \frac{1}{2}\lambda_i, \tag{52}$$

whence $z_i = \pm\sqrt{N}$. Thus there are $2N$ stationary points, each corresponding to $\pm$ the cardinal directions on the sphere in the diagonalized basis. The energy at each stationary point is real if the couplings are real, and therefore there are no complex stationary points in the ordinary 2-spin model.

Imagine for a moment that the coupling are allowed to be complex, giving the stationary points of the model complex energies and therefore potentially interesting thimble structure. Generically, the eigenvalues of the coupling matrix will have distinct imaginary parts, and there will be no Stokes lines. Suppose that two stationary points are brought to the same imaginary energy by some continuation; without loss of generality, assume these are associated with the first and second cardinal directions. Since the gradient is proportional to z, any components that are zero at some time will be zero at all times. The gradient flow dynamics for the two components of interest assuming all others are zero are:

$$\dot{z}_1 = -z_1^*\left(\lambda_1^* - \frac{\lambda_1^* z_1^* z_1 + \lambda_2^* z_2^* z_2}{|z_1|^2 + |z_2|^2}\right) = -(\lambda_1 - \lambda_2)^* z_1^* \frac{|z_2|^2}{|z_1|^2 + |z_2|^2}, \tag{53}$$

and the same for z_2 with all indices swapped. Since $\Delta = \lambda_1 - \lambda_2$ is real when the energies and therefore eigenvalues have the same imaginary part, if z_1 begins real it remains real, with the same for z_2. Since the stationary points are at real z, we make this restriction, and find:

$$\frac{d}{dt}\left(z_1^2 + z_2^2\right) = 0 \qquad \frac{d}{dt}\frac{z_2}{z_1} = \Delta\frac{z_2}{z_1}. \tag{54}$$

Therefore $z_2/z_1 = e^{\Delta t}$, with $z_1^2 + z_2^2 = N$ as necessary. Depending on the sign of Δ, z flows from one stationary point to the other over infinite time. This is a Stokes line, and establishes that any two distinct stationary points in the 2-spin model with the same imaginary energy will possess one. These trajectories are plotted in figure 10.
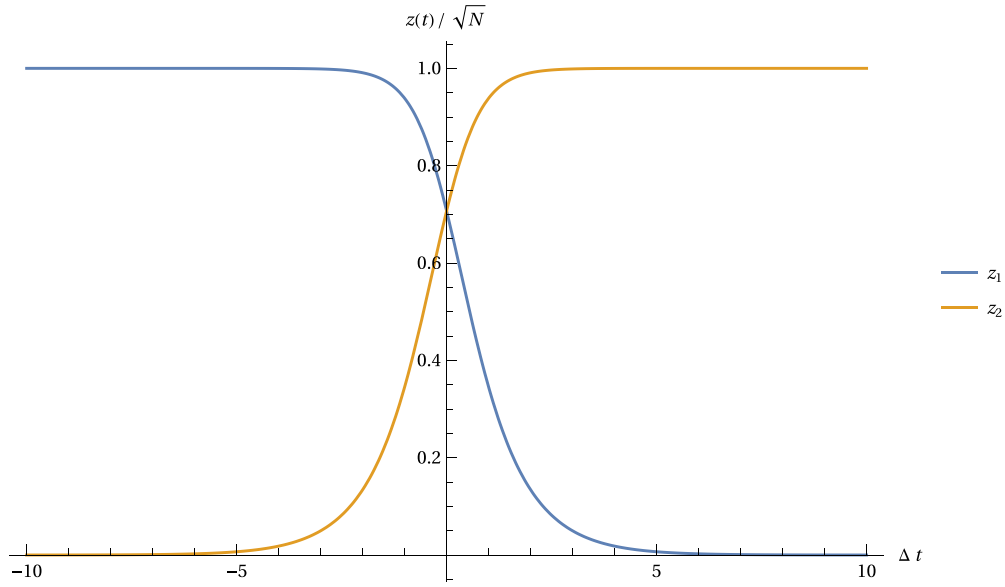
Figure 10. The Stokes line in the 2-spin model when the stationary points associated with the first and second cardinal directions are brought to the same imaginary energy. Δ is proportional to the difference between the real energies of the first and the second stationary point; when $\Delta > 0$ flow is from first to second, while when $\Delta < 0$ it is reversed.

Since they sit at the corners of a simplex, the distinct stationary points of the 2-spin model are all adjacent: no stationary point is separated from another by the separatrix of a third. This means that when the imaginary energies of two stationary points are brought to the same value, their surfaces of constant imaginary energy join. However, this is not true for stationary points related by the symmetry $z \rightarrow -z$, as seen in figure 7.

Since the 2-spin model with real couplings does not have any stationary points in the complex plane, analytic continuation can be made without any fear of running into Stokes points. Starting from real, large β, making an infinitesimal phase rotation into the complex plane results in a decomposition into thimbles where that of each stationary point is necessary, because all stationary points are real and their antithimbles all intersect the real sphere. The curvature of the action at the stationary point lying at $z_i = \sqrt{N}\delta_{ik}$ in the jth direction is given by $\lambda_k - \lambda_j = 2(\epsilon_k - \epsilon_j)$. Therefore the generic case of N distinct eigenvalues of the coupling matrix leads to $2N$ stationary points with N distinct energies, two at each index from 0 to $D = N - 1$. Starting with the expression (32), we have:

$$
\begin{aligned}
Z &= \int_{S^{N-1}} ds\, e^{-\beta \mathcal{S}_2(s)} = \sum_{\sigma \in \Sigma_0} n_\sigma \int_{\mathcal{J}_\sigma} ds\, e^{-\beta \mathcal{S}_2(s)} \\
&\simeq \sum_{\sigma \in \Sigma_0} i^{k_\sigma} \left(\frac{2\pi}{\beta}\right)^{D/2} e^{-\beta \mathcal{S}_2(s_\sigma)} |\det \mathrm{Hess}\, \mathcal{S}_2(s_\sigma)|^{-\frac{1}{2}} \\
&= 2\sum_{k=0}^{D} \exp\left\{ i\frac{\pi}{2}k + \frac{D}{2}\log\frac{2\pi}{\beta} - N\beta\epsilon_k - \frac{1}{2}\sum_{\ell \neq k}\log 2|\epsilon_k - \epsilon_\ell| \right\},
\end{aligned}
\tag{55}
$$

where ε_k is the energy of the twin stationary points of index k. In the large N limit, we take advantage of the limiting distribution ρ of these energies to write:

$$\overline{Z} \simeq 2 \int d\epsilon \, \rho(\epsilon) \exp\left\{ i\frac{\pi}{2}k_\epsilon + \frac{D}{2}\log\frac{2\pi}{\beta} - N\beta\epsilon - \frac{D}{2}\int d\epsilon' \, \rho(\epsilon')\log 2|\epsilon - \epsilon'| \right\}$$
$$= 2 \int d\epsilon \, \rho(\epsilon) e^{Nf(\epsilon)}, \tag{56}$$

since the J of the 2-spin model is a symmetric real matrix with variance $1/N$, its eigenvalues are distributed by a semicircle distribution of radius 2, and therefore the energies ε are distributed by a semicircle distribution of radius one, with:

$$\rho(\epsilon) = \frac{2}{\pi}\sqrt{1 - \epsilon^2}. \tag{57}$$

The index as a function of energy level is given by the cumulative density function:

$$k_\epsilon = D \int_{-\infty}^{\epsilon} d\epsilon' \, \rho(\epsilon') = \frac{D}{\pi}\left(\epsilon\sqrt{1^2 - \epsilon^2} + 2\tan^{-1}\frac{1+\epsilon}{\sqrt{1-\epsilon^2}} \right). \tag{58}$$

Finally, the product over the singular values corresponding to descending directions gives:

$$\frac{1}{2}\int d\epsilon' \, \rho(\epsilon')\log 2|\epsilon - \epsilon'| = -\frac{1}{4} + \frac{1}{2}\epsilon^2, \tag{59}$$

for $\epsilon^2 < 1$. This gives the function f in the exponential as:

$$\mathrm{Re}f = -\epsilon\,\mathrm{Re}\,\beta + \frac{1}{4} - \frac{1}{2}\epsilon^2, \tag{60}$$

$$\mathrm{Im}f = -\epsilon\,\mathrm{Im}\,\beta + \frac{1}{2}\left(\epsilon\sqrt{1-\epsilon^2} + 2\tan^{-1}\frac{1+\epsilon}{\sqrt{1-\epsilon^2}} \right). \tag{61}$$

The value of the integral will be dominated by the contribution near the maximum of the real part of f, which is:

$$\epsilon_{\max} = \begin{cases} -\mathrm{Re}\,\beta & \mathrm{Re}\,\beta \leqslant 1 \\ -1 & \text{otherwise} \end{cases} \tag{62}$$

For $\mathrm{Re}\,\beta > 1$, the maximum is concentrated in the ground state and the real part of f comes to a cusp, meaning that the oscillations do not interfere in taking the saddle point. Once this line is crossed and the maximum enters the bulk of the spectrum, one expects to find cancellations caused by the incoherent contributions of thimbles with nearby energies to $\epsilon_{\max}$. Therefore, one expects that $\overline{Z}$ enters a phase with no coherent average when $\mathrm{Re}\,\beta = 1$.

On the other hand, there is another point where the thimble sum becomes coherent. This is when the oscillation frequency near the maximum energy goes to zero. This happens for:

$$0 = \frac{\partial}{\partial\epsilon}\mathrm{Im}f\bigg|_{\epsilon=\epsilon_{\max}} = -\mathrm{Im}\,\beta + \sqrt{1 - \epsilon_{\max}^2} = -\mathrm{Im}\,\beta + \sqrt{1 - (\mathrm{Re}\,\beta)^2}, \tag{63}$$

or for $|\beta| = 1$. Here the sum of contributions from thimbles near the maximum again becomes coherent, because the period of oscillations in ε diverges at the maximum. These conditions correspond precisely to the phase boundaries of the density of zeros in the 2-spin model found previously using other methods [9, 10].

We've seen that even in the 2-spin model, which is not complex, making a thimble decomposition in a theory with many saddles does not necessarily fix the sign problem. Instead, it takes a potentially high-dimensional sign problem and produces a one-dimensional one, represented by the oscillatory integral over $e^{Nf(\epsilon)}$. In some regimes, it can be argued that integral

has a maximum with a coherent neighborhood, allowing computation to be made. In others, oscillations in the phase remain, from the sum over the many thimbles. We will find a similar story for the pure p-spin models for $p > 2$ in the next sections, complicated by the additional presence of Stokes points in the continuation.

4.2. Pure p-spin: where are the saddles?

We studied the distribution of stationary points in the pure p-spin models in previous work [6]. Here, we will review the method and elaborate on some of the results relevant to analytic continuation.

The complexity of the real p-spin models has been studied extensively, and is even known rigorously [11]. If $\mathcal{N}(\epsilon)$ is the number of stationary points with specific energy ε, then the complexity is defined by:

$$\Sigma(\epsilon) = \lim_{N \to \infty} \frac{1}{N} \log \overline{\mathcal{N}}(\epsilon), \tag{64}$$

a natural measure of how superextensive the average number $\overline{\mathcal{N}} \sim e^{N\Sigma}$ is. The complexity is also known for saddles of particular index, with, e.g. $\Sigma_{k=1}$ measuring the complexity of rank-one saddles and $\Sigma_{k=0}$ measuring that of minima. The minimum energy for which $\Sigma_{k=0}$ is positive corresponds to the ground state energy of the model, because at large N below this the number of minima is expected to be exponentially small with N. We'll write the ground state energy as $\epsilon_{k=0}$, and the lowest energies at which rank j saddles are found as $\epsilon_{k=j}$, so that, e.g.:

$$0 = \Sigma(\epsilon_{k=0}) = \Sigma_{k=0}(\epsilon_{k=0}) \qquad 0 = \Sigma_{k=1}(\epsilon_{k=1}). \tag{65}$$

In the real case, the p-spin models possess a threshold energy:

$$|\epsilon_{\text{th}}|^2 = \frac{2(p-1)}{p}, \tag{66}$$

below which there are exponentially many minima compared to saddles, and above which vice versa. This threshold persists in a more generic form in the complex case, where now the threshold separates stationary points that have mostly gapped from mostly ungapped spectra. Since the p-spin model has a hessian that consists of a symmetric complex matrix with a shifted diagonal, we can use the results of section 2.4. The variance of the p-spin hessian without shift is:

$$\overline{|\partial\partial\mathcal{S}_p|^2} = \frac{p(p-1)\left(\frac{1}{N}z^\dagger z\right)^{p-2}}{2N} = \frac{p(p-1)}{2N}(1+2Y)^{p-2}, \tag{67}$$

$$\overline{(\partial\partial\mathcal{S}_p)^2} = \frac{p(p-1)\left(\frac{1}{N}z^T z\right)^{p-2}}{2N} = \frac{p(p-1)}{2N}, \tag{68}$$

where $Y = \frac{1}{N}\|\operatorname{Im} z\|^2$ is a measure of how far the stationary point is into the complex configuration space. As expected for a real problem, the two variances coincide when $Y = 0$. The diagonal shift is $-p\epsilon$. In the language of section 2.4, this means that $\Gamma_0 = p(p-1)(1+2Y)^{p-2}/2$, $C_0 = p(p-1)/2$, and $\lambda_0 = -p\epsilon$. This means that the energy at which the gap appears is, using (43):

$$|\epsilon_{\text{gap}}|^2 = \frac{p-1}{2p}\frac{[1-(1+2Y)^{2(p-2)}]^2(1+2Y)^{p-2}}{1+(1+2Y)^{2(p-2)}-2(1+2Y)^{p-2}\cos(2\arg\epsilon)}. \tag{69}$$

When ε is real, $\lim_{Y\to 0}|\epsilon_{\text{gap}}| = |\epsilon_{\text{th}}|$.

The complexity of stationary points by their energy and location Y can be determined by the Kac–Rice formula. Any stationary point of the action is a stationary point of the real part of the action, and we can write:

$$\mathcal{N} = \int dx\,dy\,\delta(\partial_x \operatorname{Re} \tilde{\mathcal{S}}_p)\delta(\partial_y \operatorname{Re} \tilde{\mathcal{S}}_p)\,|\det \operatorname{Hess}_{x,y} \operatorname{Re} \mathcal{S}_p|. \tag{70}$$

This expression is to be averaged over J to give the complexity Σ as $N\Sigma = \overline{\log \mathcal{N}}$, a calculation that involves the replica trick. Based on the experience from similar problems [12], the *annealed approximation* $N\Sigma \sim \log \overline{\mathcal{N}}$ is expected to be exact wherever the complexity is positive.

As in section 2.4, this expression can be bright into a manifestly complex form using Cauchy–Riemann relations. This gives:

$$\mathcal{N} = \int dz^* dz\,d\hat{z}^* d\hat{z}\,d\eta^* d\eta\,d\gamma^* d\gamma \exp\left\{ \operatorname{Re}\left(\hat{z}^T \partial \tilde{\mathcal{S}}_p + \eta^T \partial\partial \tilde{\mathcal{S}}_p \gamma\right)\right\}, \tag{71}$$

where η and γ are N-dimensional Grassmann fields. This can be more conveniently studied using the method of superfields. For an overview of superfields applied to the p-spin spherical models, see [13]. Our previous work deriving the complexity does not use superfields [6], but they will be essential for compactly writing the *two* replica complexity in the next section, and so we briefly introduce the technique here. Introducing the one-component Grassmann variables θ and $\bar{\theta}$, define the superfield:

$$\phi(1) = z + \bar{\theta}(1)\eta + \gamma\theta(1) + \hat{z}\bar{\theta}(1)\theta(1), \tag{72}$$

and its measure $d\phi = dz\,d\hat{z}\,d\eta\,d\gamma$. Then the expression for the number of stationary points can be written in a compact form, as:

$$\mathcal{N} = \int d\phi^* d\phi \exp\left\{\int d1 \operatorname{Re} \tilde{\mathcal{S}}_p(\phi(1))\right\}, \tag{73}$$

where $d1 = d\bar{\theta}(1)\,d\theta(1)$ denotes the integration over the Grassmann variables. This can be related to the previous expression by expansion with respect to the Grassmann variables, recognizing that $\theta^2 = \bar{\theta}^2 = 0$ restricts the series to two derivatives.

From here the process can be treated as usual, averaging over the couplings and replacing bilinear combinations of the fields with their own variables via a Hubbard–Stratonovich transformation. Defining the supermatrix:

$$Q(1,2) = \frac{1}{N}\begin{bmatrix} \phi(1)^T\phi(2) & \phi(1)^T\phi(2)^* \\ \phi(1)^\dagger\phi(2) & \phi(1)^\dagger\phi(2)^* \end{bmatrix}, \tag{74}$$

the result can be written, neglecting constant factors, as an integral over Q like:

$$\overline{\mathcal{N}} \simeq \int dQ\,e^{NS_{\text{eff}}(Q)}, \tag{75}$$

where the effective action functional S_{eff} of the supermatrix Q is:

$$S_{\text{eff}} = \int d1\,d2\operatorname{Tr}\left(\frac{1}{4}\begin{bmatrix} \frac{1}{4} & \frac{1}{4} \\ \frac{1}{4} & \frac{1}{4} \end{bmatrix} Q^{(p)}(1,2) - \frac{p}{2}\begin{bmatrix} \frac{\epsilon}{2} & 0 \\ 0 & \frac{\epsilon^*}{2} \end{bmatrix}(Q(1,1) - I)\delta(1,2)\right)$$
$$+ \frac{1}{2}\log\det Q. \tag{76}$$

The exponent in parentheses denotes element-wise exponentiation, and:

$$\delta(1,2) = (\bar{\theta}(1) - \bar{\theta}(2))(\theta(1) - \theta(2)), \tag{77}$$

is the superspace δ-function, and the determinant and trace are a superdeterminant and super-trace, respectively. Algebraically and under calculus they behave nearly like their non-super counterparts. This leads to the condition for a saddle point of:

$$0 = \frac{\partial S_{\text{eff}}}{\partial Q(1,2)} = \frac{p}{16}Q^{(p-1)}(1,2) - \frac{p}{2}\begin{bmatrix} \frac{\epsilon}{2} & 0 \\ 0 & \frac{\epsilon^*}{2} \end{bmatrix}\delta(1,2) + \frac{1}{2}Q^{-1}(1,2), \quad (78)$$

where the inverse supermatrix is defined by:

$$I\delta(1,2) = \int d3\, Q^{-1}(1,3)Q(3,2). \quad (79)$$

Convolving both sides by another supermatrix to remove the inverse, we arrive at the saddle point equations:

$$\begin{aligned}
0 &= \int d3\, \frac{\partial S_{\text{eff}}}{\partial Q(1,3)}Q(3,2) \\
&= \frac{p}{16}\int d3\, Q^{(p-1)}(1,3)Q(3,2) - \frac{p}{2}\begin{bmatrix} \frac{\epsilon}{2} & 0 \\ 0 & \frac{\epsilon^*}{2} \end{bmatrix}Q(1,2) + \frac{1}{2}I\delta(1,2).
\end{aligned} \quad (80)$$

When expanded, the supermatrix Q contains nine independent bilinear combinations of the original variables: $z^\dagger z$, $\hat{z}^T z$, $\hat{z}^\dagger z$, $\hat{z}^T \hat{z}$, $\hat{z}^\dagger \hat{z}$, $\eta^\dagger \eta$, $\gamma^\dagger \gamma$, $\eta^\dagger \gamma$, and $\eta^T \gamma$. The saddle point equations can be used to eliminate all but one of these, the 'radius' like term $z^\dagger z$. When combined with the constraint, this term can be related directly to the magnitude of the imaginary part of z, since $z^\dagger z = x^T x + y^T y = N + 2y^T y = N(1 + 2Y)$ for $Y = \|\text{Im}\,z\|^2/N = y^T y/N$. The complexity can then be written in terms of $r = z^\dagger z/N = 1 + 2Y$ as:

$$\Sigma = \log(p-1) - \frac{1}{2}\log\left(\frac{1 - r^{-2(p-1)}}{1 - r^{-2}}\right) - \frac{(\text{Re}\,\epsilon)^2}{R_+^2} - \frac{(\text{Im}\,\epsilon)^2}{R_-^2} + I_p(\epsilon/|\epsilon_{\text{th}}|), \quad (81)$$

where

$$R_\pm^2 = \frac{p-1}{2}\frac{(r^{p-2} \pm 1)\left[r^{2(p-1)} \pm (p-1)r^{p-2}(r^2 - 1) - 1\right]}{1 + r^{2(p-2)}\left[p(p-2)(r^2 - 1) - 1\right]}, \quad (82)$$

and the function $I_p(u) = 0$ if $|\epsilon|^2 < |\epsilon_{\text{gap}}|^2$ and:

$$\begin{aligned}
I_p(u) &= \left(\frac{1}{2} + \frac{1}{r^{p-2} - 1}\right)^{-1}(\text{Re}\,u)^2 - \left(\frac{1}{2} - \frac{1}{r^{p-2} + 1}\right)^{-1}(\text{Im}\,u)^2 \\
&\quad - \log\left(r^{p-2}\left|u + \sqrt{u^2 - 1}\right|^2\right) + 2\,\text{Re}\left(u\sqrt{u^2 - 1}\right)
\end{aligned}, \quad (83)$$

otherwise. The branch of the square roots are chosen such that the real part of the root has the opposite sign as the real part of u, e.g. if $\text{Re}\,u < 0$ then $\text{Re}\,\sqrt{u^2 - 1} > 0$. If the real part is zero, then the sign is taken so that the imaginary part of the root has the opposite sign of the imaginary part of u.

Contours of this complexity for the pure 3-spin are plotted in figure 11 for pure real and imaginary energy. The thick black line shows the contour of zero complexity, where stationary points are no longer found at large N. As the magnitude of the imaginary part of the spin taken greater, more stationary points are found, and at a wider array of energies. This is also true in other directions into the complex energy plane, where the story is qualitatively the same. At any energy, the limit $Y \to \infty$ or $r \to \infty$ results in $\Sigma = \log(p-1)$, which saturates the Bézout bound on the number of stationary points a polynomial of order p can have [14].

Something more interesting is revealed if we zoom in on the complexity around the ground state, shown in figure 12. Here, the region where most stationary points have a gapped hessian
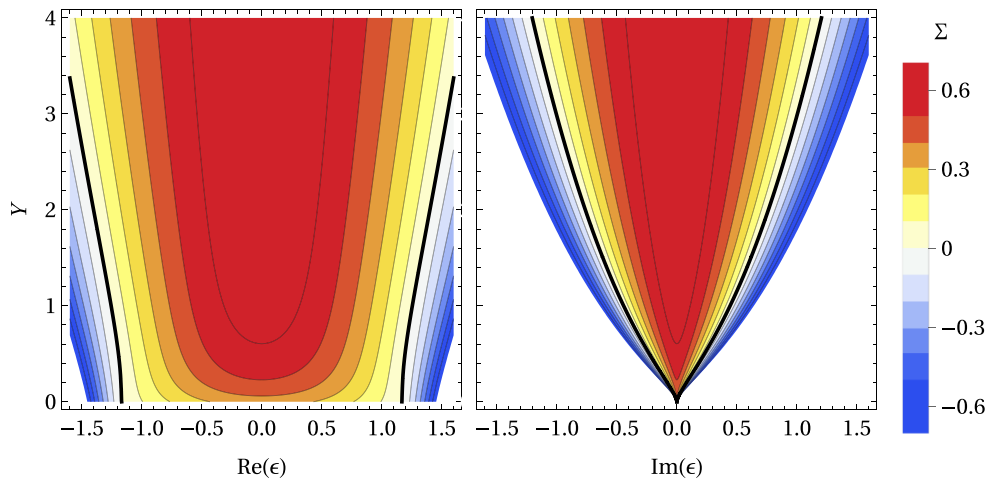
Figure 11. The complexity of the 3-spin spherical model in the complex plane, as a function of pure real and imaginary energy (left and right) and the magnitude $Y = \|\operatorname{Im} z\|^2 / N$ of the distance into the complex configuration space. The thick black contour shows the line of zero complexity, where stationary points become exponentially rare in N.
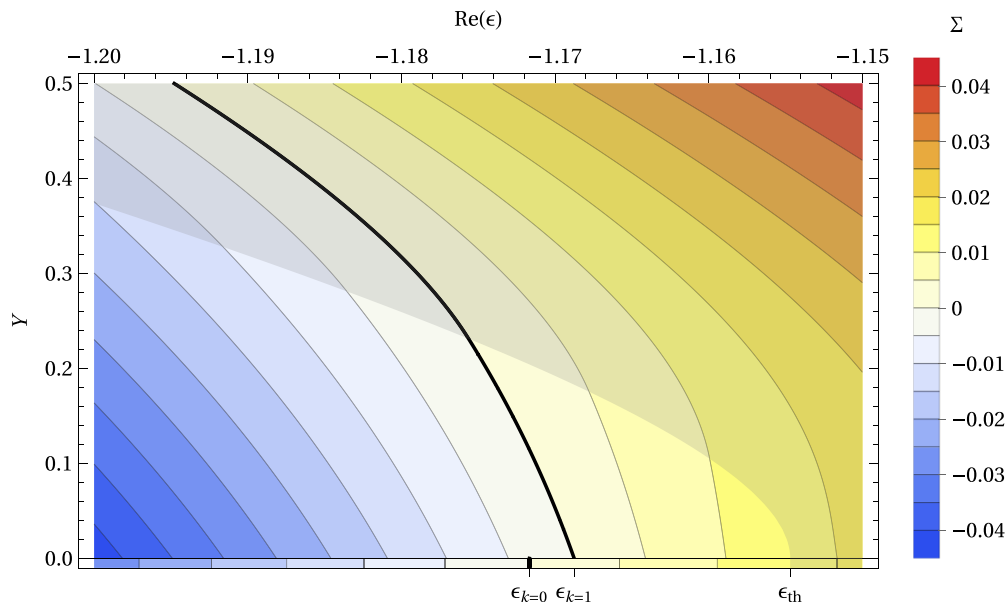
Figure 12. The complexity of the 3-spin spherical model in the complex plane, as a function of pure real energy and the magnitude $Y = \|\operatorname{Im} z\|^2 / N$ of the distance into the complex configuration space. The thick black contour shows the line of zero complexity, where stationary points become exponentially rare in N. The shaded region shows where stationary points have an ungapped spectrum. The complexity of the 3-spin model on the real sphere is shown below the horizontal axis; notice that it does not correspond with the limiting complexity in the complex configuration space below the threshold energy.

is shaded. The line ϵ_{gap} separating gapped from ungapped spectra corresponds to the threshold energy ϵ_{th} in the limit of $Y \to 0$. Above the threshold, the limit of the complexity as $Y \to 0$ (or equivalently $r \to 1$) also approaches the real complexity, plotted under the horizontal axis. However, below the threshold this is no longer the case: here the limit of $Y \to 0$ of the complexity of complex stationary points corresponds to the complexity $\Sigma_{k=1}$ of *rank one saddles* in the real problem, and their complexity becomes zero at $\epsilon_{k=1}$, where the complexity of rank one saddles becomes zero [11].

There are several interesting features of the complexity. First is this inequivalence between the real complexity and the limit of the complex complexity to zero complex part. It implies, among other things, a desert of stationary points in the complex plan surrounding the lowest minima, something we shall see more explicitly in the next section. Second, there is only a small collection of stationary points that appear with positive complexity and a gapped spectrum: the small region in figure 12 that is both to the right of the thick line and brightly shaded. We suspect that these are the only stationary points that have any hope of avoiding participation in Stokes points.

4.3. Pure p-spin: where are my neighbors?

The problem of counting the density of Stokes points in an analytic continuation of the spherical models is quite challenging, as the problem of finding dynamic trajectories with endpoints at stationary points is already difficult, and once made complex the problem has twice the number of fields squared.

In this section, we begin to address the problem heuristically by instead asking: if you are at a stationary point, where are your neighbors? The stationary points geometrically nearest to a given stationary point should make up the bulk of its adjacent points in the sense of being susceptible to Stokes points. The distribution of these near neighbors in the complex configuration space therefore gives a sense of whether many Stokes lines should be expected, and when.

To determine this, we perform the same Kac–Rice procedure as in the previous section, but now with two probe points, or replicas, of the system. The simplify things somewhat, we will examine the case where the only second probe is complex; the first probe will be on the real sphere. The number of stationary points with given energies $\epsilon_1 \in \mathbb{R}$ and $\epsilon_2 \in \mathbb{C}$ are, in the superfield formulation,

$$\mathcal{N}^{(2)} = \int d\phi_1 \, d\phi_2^* \, d\phi_2 \exp\left\{ \int d1 \left[\tilde{\mathcal{S}}_p(\phi_1(1)) + \operatorname{Re}\tilde{\mathcal{S}}_p(\phi_2(1)) \right] \right\}, \qquad (84)$$

and we expect to find a two-spin complexity counting pairs of the form:

$$\Sigma^{(2)} = \lim_{N \to \infty} \frac{1}{N} \log \mathcal{N}^{(2)}, \qquad (85)$$

which depends on the two energies and on mutual geometric invariants of the two probe points. The calculation follows exactly as before, but with an additional field. The average over J is taken, and the supermatrix:

$$Q(1,2) = \begin{bmatrix} \phi_1(1)^T\phi_1(2) & \phi_1(1)^T\phi_2(2) & \phi_1(1)^T\phi_2(2)^* \\ \phi_2(1)^T\phi_1(2) & \phi_2(1)^T\phi_2(2) & \phi_2(1)^T\phi_2(2)^* \\ \phi_2(1)^\dagger\phi_1(2) & \phi_2(1)^\dagger\phi_2(2) & \phi_2(1)^\dagger\phi_2(2)^* \end{bmatrix}, \qquad (86)$$

is inserted with a Hubbard–Stratonovich transformation. The average number of pairs can then be written in the form:

$$\overline{\mathcal{N}^{(2)}} \propto \int dQ \, e^{NS_{\text{eff}}[Q]}, \tag{87}$$

for the effective action:

$$
S_{\text{eff}} = \int d1 \, d2 \, \text{Tr} \left\{ \frac{1}{4} \begin{bmatrix} 1 & \frac{1}{2} & \frac{1}{2} \\ \frac{1}{2} & \frac{1}{4} & \frac{1}{4} \\ \frac{1}{2} & \frac{1}{4} & \frac{1}{4} \end{bmatrix} Q^{(p)}(1,2) \right.
$$
$$
\left. - \frac{p}{2} \begin{bmatrix} \epsilon_1 & 0 & 0 \\ 0 & \frac{1}{2}\epsilon_2 & 0 \\ 0 & 0 & \frac{1}{2}\epsilon_2^* \end{bmatrix} (Q(1,1) - I) \, \delta(1,2) \right\} + \frac{1}{2} \det Q. \tag{88}
$$

Differentiating this with respect to Q, one finds the saddle point equations:

$$
0 = \frac{\partial S_{\text{eff}}}{\partial Q(1,2)} = \frac{p}{4} \begin{bmatrix} 1 & \frac{1}{2} & \frac{1}{2} \\ \frac{1}{2} & \frac{1}{4} & \frac{1}{4} \\ \frac{1}{2} & \frac{1}{4} & \frac{1}{4} \end{bmatrix} \odot Q^{(p-1)}(1,2)
$$
$$
- \frac{p}{2} \begin{bmatrix} \epsilon_1 & 0 & 0 \\ 0 & \frac{1}{2}\epsilon_2 & 0 \\ 0 & 0 & \frac{1}{2}\epsilon_2^* \end{bmatrix} \delta(1,2) + \frac{1}{2} Q^{-1}(1,2), \tag{89}
$$

where $\odot$ denotes element-wise multiplication. These are simplified by convolution to remove the superinverse, finally giving:

$$
0 = \int d3 \frac{\partial S_{\text{eff}}}{\partial Q(1,3)} Q(3,2)
$$
$$
= \frac{p}{4} \int d3 \left\{ \begin{bmatrix} 1 & \frac{1}{2} & \frac{1}{2} \\ \frac{1}{2} & \frac{1}{4} & \frac{1}{4} \\ \frac{1}{2} & \frac{1}{4} & \frac{1}{4} \end{bmatrix} \odot Q^{(p-1)}(1,3) \right\} Q(3,2)
$$
$$
- \frac{p}{2} \begin{bmatrix} \epsilon_1 & 0 & 0 \\ 0 & \frac{1}{2}\epsilon_2 & 0 \\ 0 & 0 & \frac{1}{2}\epsilon_2^* \end{bmatrix} Q(1,2) + \frac{1}{2} I \delta(1,2). \tag{90}
$$

Despite being able to pose the saddle point problem in a compact way, a great deal of complexity lies within. The supermatrix Q depends on 35 independent bilinear products, and when the superfields are expanded produces 48 (not entirely independent) equations. These equations can be split into 30 involving bilinear products of the fermionic fields and 18 without them. The 18 equations without fermionic bilinear products can be solved with a computer algebra package to eliminate 17 of the 20 non-fermionic bilinear products. The fermionic equations are unfortunately more complicated.

They can be simplified somewhat by examination of the real two-replica problem. There, all bilinear products involving fermionic fields from different replicas, like $\eta_1^T \eta_2$, vanish. This is related to the influence of the relative position of the two replicas to their spectra, with the vanishing being equivalent to having no influence, i.e. the value of the determinant at each stationary point is exactly what it would be in the one-replica problem with the same invariants,

e.g. energy and radius. Making this ansatz, the equations can be solved for the remaining 5 bilinear products, eliminating all the fermionic fields.

This leaves two bilinear products: $z_2^\dagger z_2$ and $z_2^\dagger z_1$, or one real and one complex number. The first is the radius of the complex saddle, while the other is a complex generalization of the overlap. For us, it will be more convenient to work in terms of the difference $\Delta z = z_2 - z_1$ and the constants which characterize it, which are $\Delta = \Delta z^\dagger \Delta z / N = \|\Delta z\|^2 / N$ and $\gamma = \frac{\Delta z^T \Delta z}{\|\Delta z\|}$. Once again we have one real (and strictly positive) variable Δ and one complex variable γ.

Though the value of γ is bounded by $|\gamma| \leqslant 1$ as a result of the inequality $|\Delta z^T \Delta z| \leqslant \|\Delta z\|^2$, in reality this bound is not the relevant one, because we are confined on the manifold $N = z^T z$. The relevant bound is most easily established by returning to a $2N$-dimensional real problem, with $x = x_1$ and $z = x_2 + iy_2$. The constraint gives $x_2^T y_2 = 0$, $x_1^T x_1 = 1$, and $x_2^T x_2 = 1 + y_2^T y_2$. Then, by their definitions:

$$\Delta = 1 + x_2^T x_2 + y_2^T y_2 - 2x_1^T x_2 = 2(1 + y_2^T y_2 - x_1^T x_2). \tag{91}$$

Define θ_{xx} as the angle between x_1 and x_2. Then $x_1^T x_2 = \|x_1\| \|x_2\| \cos \theta_{xx} = \sqrt{1 - \|y_2\|} \cos \theta_{xx}$, and:

$$\Delta = 2\left(1 + \|y_2\|^2 - \sqrt{1 - \|y_2\|^2} \cos \theta_{xx}\right). \tag{92}$$

The definition of γ likewise gives:

$$\gamma \Delta = 2 - 2x_1^T x_2 - 2ix_1^T y_2 = 2(1 - \|x_2\| \cos \theta_{xx} - i\|y_2\| \cos \theta_{xy})$$
$$= 2\left(1 - \sqrt{1 - \|y_2\|^2} \cos \theta_{xx} - i\|y_2\| \cos \theta_{xy}\right), \tag{93}$$

where θ_{xy} is the angle between x_1 and y_2. There is also an inequality between the angles θ_{xx} and θ_{xy} between x_1 and x_2 and y_2, respectively, which takes that form $\cos^2 \theta_{xy} + \cos^2 \theta_{xx} \leqslant 1$. This results from the fact that x_2 and y_2 are orthogonal, a result of the constraint. These equations along with the inequality produce the required bound on $|\gamma|$ as a function of Δ and $\arg \gamma$, which is plotted in figure 13.

A lot of information is contained in the full two-replica complexity, but we will focus on the following question: what does the population of stationary points nearby a given real stationary point look like? We think this is a relevant question for the tendency for Stokes lines, for the following reason. To determine whether two given stationary points, when tuned to have the same imaginary energy, will share a Stokes line, one needs to solve what is known as the global connection problem. As we have seen in section 2.3, this as a question of a kind of topological adjacency: two points will *not* share a Stokes line if a third intervenes with its thimble between them. We reason that the number of adjacent stationary points of a given stationary point for a generic function in D complex dimensions scales algebraically with D. Therefore, if the collection of nearest neighbors has a nonzero complexity, i.e. scales *exponentially* with D, crowding around the stationary point in question, then these might be expected to overwhelm the possible adjacencies, and so doing simplify the problem of determining the properties of the true adjacencies. Until the nonlinear flow equations are solved with dynamical mean field theory as has been done for instantons [15], this is the best heuristic.

For all displacements Δ and real energies ε_1, the maximum complexity is found for some real values of ε_2 and γ. Therefore we can restrict our study of the most common neighbors to this. Note that the real part of γ has a geometric interpretation in terms of the properties of the neighbors: if a stationary point sits in the complex configuration space near another, $\text{Re}\,\gamma$
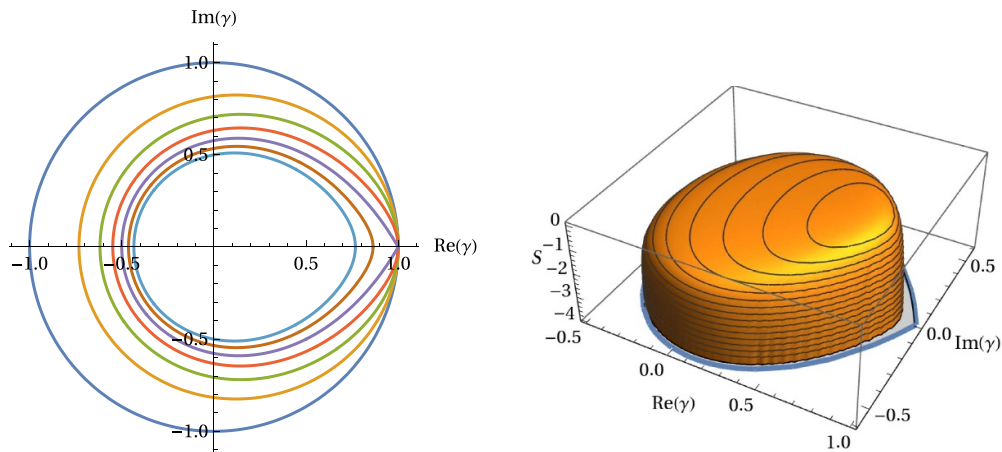
Figure 13. Left: the line bounding γ in the complex plane as a function of $\Delta = 0, 1, 2, \ldots, 6$ (outer to inner). Notice that for $\Delta \leqslant 4$, $|\gamma| = 1$ is saturated for positive real γ, but is not for $\Delta > 4$, and $\Delta = 4$ has a cusp in the boundary. This is due to $\Delta = 4$ corresponding to the maximum distance between any two points on the real sphere. Right: the two-spin complexity for $\Delta = 4$ and some energy $\epsilon_1 = \epsilon_2$. It approaches $-\infty$ at the boundary.
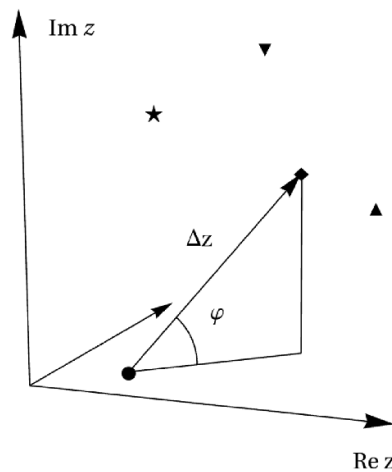

Figure 14. The geometric definition of the angle φ, between the displacement between two stationary points and the real configuration space.

can be related to the angle φ made between the vector separating these two points and the real configuration space as:

$$\varphi = \arctan \sqrt{\frac{1 - \operatorname{Re}\gamma}{1 + \operatorname{Re}\gamma}}. \tag{94}$$

The geometry described above is visualized in figure 14. Having concluded that the most populous neighbors are confined to real γ, we will make use of this angle instead of γ, which has a more direct geometric interpretation.

$\Sigma^{(2)} / \Sigma_{k \geq 2}$
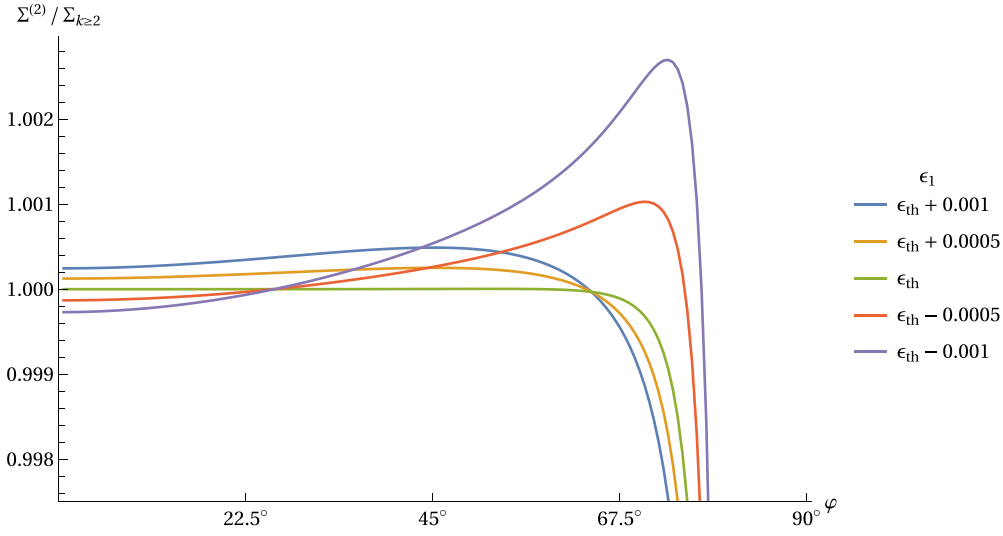
Figure 15. The scaled two-replica complexity $\Sigma^{(2)}$ as a function of angle φ with $\epsilon_2 = \epsilon_1$, $\Delta = 2^{-7}$, and various ε_1. At the threshold, the function undergoes a geometric transition and becomes sharper with decreasing Δ.
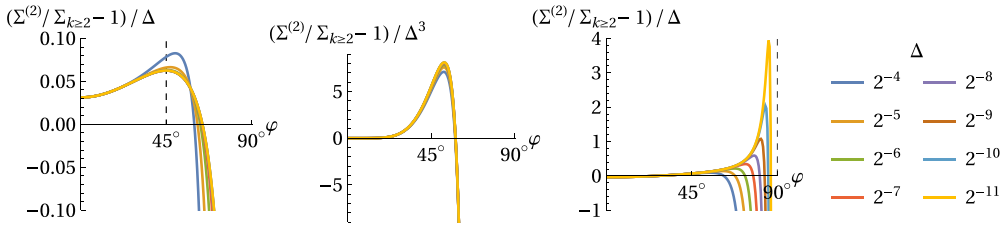
Figure 16. The scaled two-replica complexity $\Sigma^{(2)}$ as a function of angle φ for various Δ, $\epsilon_2 = \epsilon_1$, and left: $\epsilon_1 = \epsilon_{\text{th}} + 0.001$, center: $\epsilon_1 = \epsilon_{\text{th}}$, right: $\epsilon = \epsilon_{\text{th}} - 0.001$. All lines have been normalized by the complexity $\Sigma_{k \geqslant 2}$ of index 2 and greater saddles of the real 3-spin model.

First, we examine the importance of the threshold. Figure 15 shows the two-replica complexity evaluated at $\Delta = 2^{-4}$ and equal energy $\epsilon_2 = \epsilon_1$ as a function of φ for several ε_1 as the threshold is passed. The curves are rescaled by the complexity $\Sigma_{k \geqslant 2}(\epsilon_1)$ of index 2 and greater saddles in the real problem, which is what is approached in the limit as Δ to zero. Below the threshold, the distribution of nearby saddles with the same energy by angle is broad and peaked around $\varphi = 45°$, while above the threshold it is peaked strongly near the maximum φ allowed by the bound. At the threshold, the function becomes extremely flat.

One can examine the scaling of these curves as Δ goes to zero in figure 16. Both above and below the threshold, one finds a quickly-converging limit of $\left(\Sigma^{(2)} / \Sigma_{k \geqslant 2} - 1 \right) / \Delta$. Above the threshold, these curves converge to a function whose peak is always precisely at $45°$, while below they converge to a function with a peak that grows linearly with Δ^{-1} at $90°$. At the threshold, the scaling is different, and the function approaches a flat function extremely rapidly, as Δ^3.

33
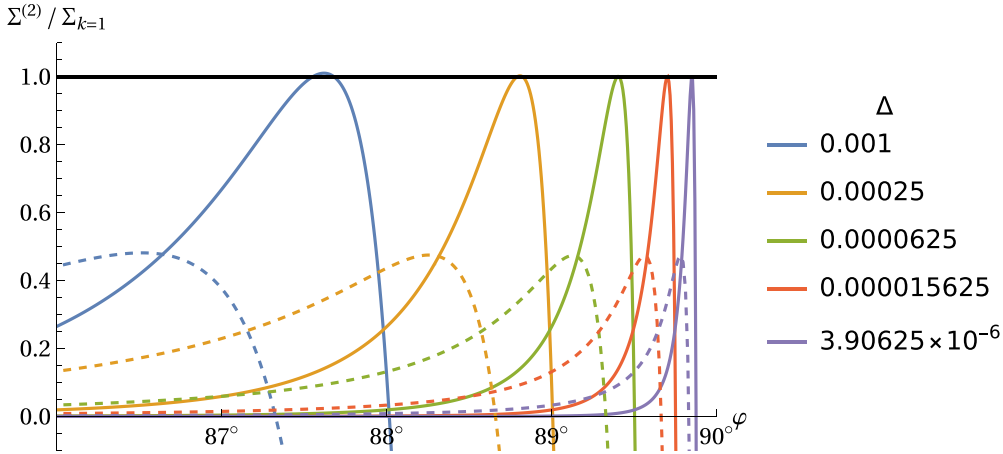
Figure 17. The two-replica complexity $\Sigma^{(2)}$ scaled by $\Sigma_{k=1}$ as a function of angle φ for various Δ at $\epsilon_1 = \epsilon_{k=2}$, the point of zero complexity for rank-two saddles in the real problem. Solid lines: the complexity evaluated at the value of ε_2 which leads to the largest maximum value. As Δ varies this varies like $\epsilon_2 - \epsilon_1 \propto \Delta^2$. Dashed lines: the complexity evaluated at $\epsilon_2 = \epsilon_1$.

Thus, there is an abrupt geometric transition in the population of nearest neighbors as the threshold is crossed: above they are broadly distributed at all angles, while below they are highly concentrated around $90°$. From this analysis it appears that the complexity of the nearest neighbors, at zero distance, behaves as that of the index-2 saddles at all angles, which would imply that the nearest neighbors vanish at the same point as the index-2 saddles. However, this is not the case: we have only shown that this is how the neighbors at *identical energy* scale, which is correct above the threshold, but no longer underneath.

If an energy is taken under the threshold and the two-replica complexity maximized with respect to both ε_2 and φ, one finds that as $\Delta \to 0$, $\epsilon_2 \to \epsilon_1$, as must be the case the find a positive complexity at zero distance, but the maximum is never at $\epsilon_2 = \epsilon_1$, but rather at a small distance $\Delta\epsilon$ that decreases with decreasing Δ like Δ^2. This is shown in figure 17. When the complexity is maximized in both parameters, one finds that, in the limit as $\Delta \to 0$, the peak is at $90°$ but has a height equal to $\Sigma_{k=1}$, the complexity of rank-1 saddles.

Below $\epsilon_{k=1}$, where the rank-1 saddle complexity vanishes, the complexity of stationary points of any type at zero distance is negative. To find what the nearest population looks like, one must find the minimum Δ at which the complexity is nonnegative, or:

$$\Delta_{\min} = \operatorname{argmin}_\Delta \left(0 \leqslant \max_{\epsilon_2, \varphi} \Sigma^{(2)}(\epsilon_1, \epsilon_2, \Delta, \varphi) \right). \tag{95}$$

The result in $\Delta_{\min}$ and the corresponding φ that produces it is plotted in figure 19. As the energy is brought below $\epsilon_{k=1}$, $\epsilon_2 - \epsilon_1 \propto -|\epsilon_1 - \epsilon_{k=1}|^2$, $\varphi - 90° \propto -|\epsilon_1 - \epsilon_{k=1}|^{1/2}$, and $\Delta_{\min} \propto |\epsilon_1 - \epsilon_{k=1}|$. The fact that the population of nearest neighbors has an energy lower than the stationary point gives some hope for the success of continuation involving these points: since Stokes points only lead to a change in weight when they involve upward flow from a point that already has weight, neighbors that have a lower energy will not be eligible to be involved in a Stokes line that causes a change of weight until the phase of β has rotated almost $180°$. The energy of nearest neighbors is plotted in figure 18, while their angular distribution and distance is plotted in figure 19.
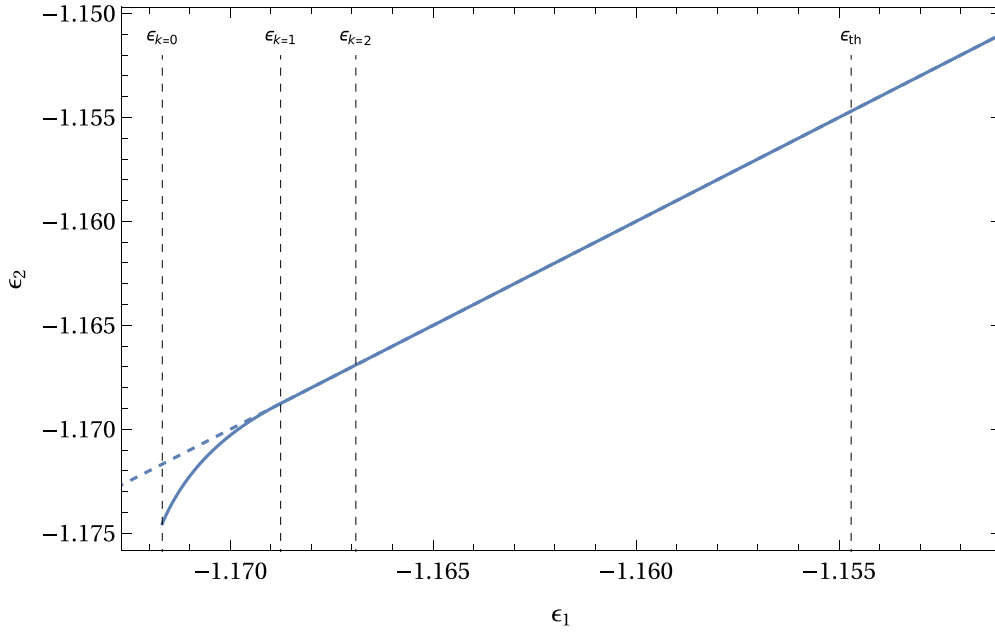
Figure 18. The energy ε_2 of the nearest neighbor stationary points in the complex plane to a given real stationary point of energy ε_1. The dashed line shows $\epsilon_2 = \epsilon_1$. The nearest neighbor energy coincides with the dashed line until $\epsilon_{k=1}$, the energy where rank-one saddles vanish, where it peels off.

4.4. Pure p-spin: numerics

To study Stokes lines numerically, we approximated them by parametric curves. If z_0 and z_1 are two stationary points of the action with $\mathrm{Re}\,\mathcal{S}(z_0) > \mathrm{Re}\,\mathcal{S}(z_1)$, then we take the curve:

$$z(t) = (1-t)z_0 + tz_1 + (1-t)t\sum_{i=0}^{m} g_i P_i^{(1,1)}(2t-1), \tag{96}$$

where the gs are undetermined complex vectors and the $P_i^{(1,1)}(x)$ are the Jacobi polynomials, orthogonal on the interval $[-1,1]$ under the weight $(1-x)(1+x)$. The Jacobi polynomials are used because they are orthogonal with respect to integration over precisely the term they appear inside above. These are fixed by minimizing a cost function, which has a global minimum only for Stokes lines. Defining:

$$\mathcal{L}(t) = 1 - \frac{\mathrm{Re}\,[\dot z(z(t))^\dagger z'(t)]}{|\dot z(z(t))||z'(t)|}, \tag{97}$$

where $\dot z(z)$ is the flow at z given by (7), this cost is given by:

$$\mathcal{C} = \int_0^1 dt\,\mathcal{L}(t), \tag{98}$$

$\mathcal{C}$ has minimum of zero, which is reached only by functions $z(t)$ whose tangent is everywhere parallel to the direction $\dot z$ of the dynamics. Therefore, functions that satisfy $\mathcal{C} = 0$ are time-reparameterized Stokes lines.
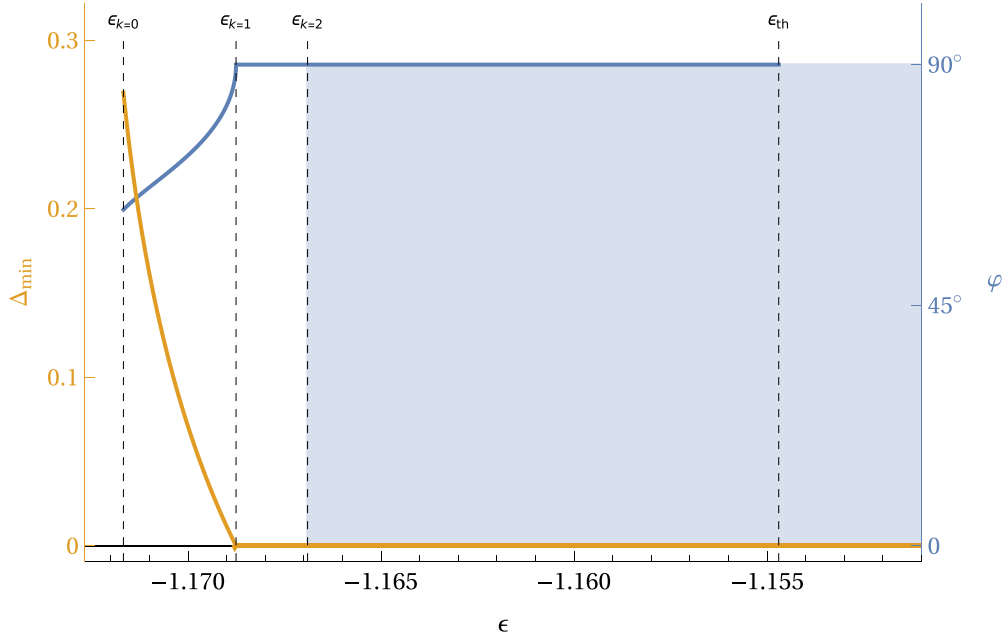
Figure 19. The properties of the nearest neighbor saddles in the 3-spin model as a function of energy ε. Above the threshold energy ϵ_{th}, stationary points are found at arbitrarily close distance and at all angles φ in the complex plane. Below ϵ_{th} but above $\epsilon_{k=2}$, stationary points are still found at arbitrarily close distance and all angles, but there are exponentially more found at $90°$ than at any other angle. Below $\epsilon_{k=2}$ but above $\epsilon_{k=1}$, stationary points are found at arbitrarily close distance but only at $90°$. Below $\epsilon_{k=1}$, neighboring stationary points are separated by a minimum squared distance $\Delta_{\min}$, and the angle they are found at drifts. The complexity of nearest neighbors in the shaded region is $\Sigma_{k\geqslant 2}$, while along the solid line for $\epsilon > \epsilon_{k=1}$ it is $\Sigma_{k=1}$. Below $\epsilon_{k=1}$ the complexity of nearest neighbors is zero.

We explicitly computed the gradient and hessian of $\mathcal{C}$ with respect to the parameter vectors g. Stokes lines are found or not between points by using the Levenberg–Marquardt algorithm starting from $g_i = 0$ for all i, and approximating the cost integral by a finite sum. To sample nearby stationary points and assess their propensity for Stokes points, we do the following. First, a saddle-finding routine based on Newton's method is run on the *real* configuration space of the *p*-spin model. Then, a saddle-finding routine is run on the complex configuration space in the close vicinity of the real saddle, using random initial conditions in a slowly increasing radius of the real stationary point. When this process finds a new distinct stationary point, it is finished. This method of sampling pairs heavily biases the statistics we report here in favor of seeing Stokes points.

Once a pair of nearby stationary points has been found, one real and one in the complex plane, their energies are used to compute the phase θ necessary to give β in order to set their imaginary energies to the same value, a necessary condition for a Stokes line. A straight line (ignoring even the constraint) is thrown between them and then minimized using the cost function (98) for some initial $m = 5$. Once a minimum is found, m is iteratively increased several times, each time minimizing the cost in between, until $m = 20$. If at some point in this process the cost blows up, indicating that the solution is running away, the pair is thrown out; this
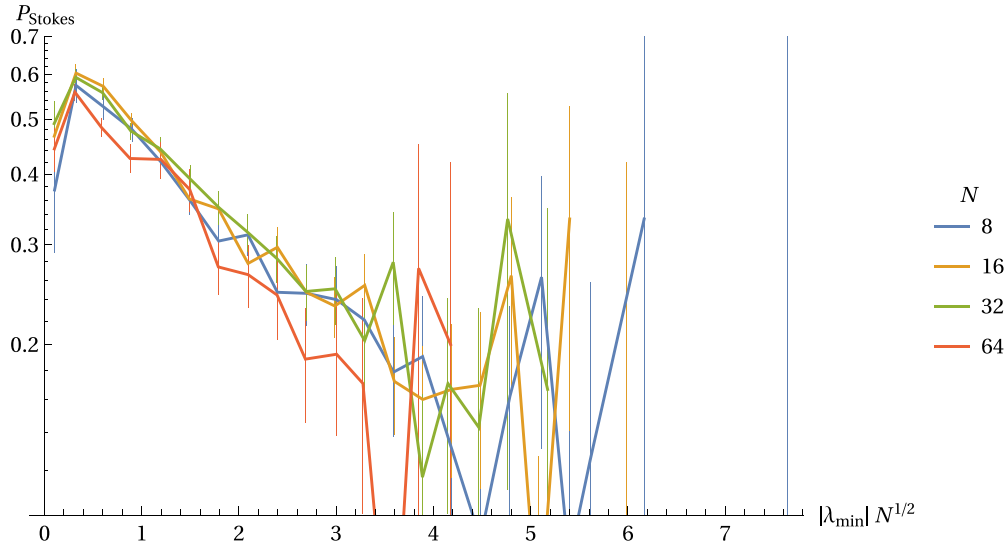
Figure 20. The probability P_{Stokes} that a real stationary point will share a Stokes line with its randomly chosen neighbor as a function of $|\lambda_{\min}|$, the magnitude of the minimum eigenvalue of the hessian at the real stationary point. The horizontal axis has been rescaled to collapse the data at different system sizes N.

happens infrequently. At the end, there are several ways to assess whether a given minimized line is a Stokes line: the value of the cost, the integrated deviation from the constraint, and the integrated deviation from constant phase. Among minimized lines these values fall into doubly-peaked histograms that well-separate prospective Stokes lines into 'good' and 'bad' values for the given level of approximation m.

One cannot explicitly study the effect of crossing various landmark energies on the p-spin in the system sizes that were accessible to our study, up to around $N = 64$, as the presence of, e.g. the threshold energy, is not noticeable until much larger size [16]. However, we are able to examine the effect of its symptoms: namely, the influence of the spectrum of the stationary point in question on the likelihood that a randomly chosen neighbor will share a Stokes line.

Data for the likelihood of a Stokes line as a function of the empirical gap $|\lambda_{\min}|$ of the real stationary point is shown in figure 20. There, one sees that the probability of finding a Stokes line with a near neighbor falls off as an exponential in the magnitude of the smallest eigenvalue. As a function of system size, the tail contracts like $N^{-1/2}$, which means that in the thermodynamic limit one expects the probability of finding such a Stokes line will approach zero everywhere expect where $\lambda_{\min} \ll 1$. This supports the idea that gapped minima are unlikely to see Stokes lines.

We can also see that as the empirical gap is increased, Stokes points tend to occur at very large phases. This can be seen for $N = 32$ in figure 21, which shows the probability distribution of Stokes lines discovered as a function of phase $|\theta|$ necessary to reach them. The curves are broken into sets representing different bins of the empirical gap $|\lambda_{\min}|$. As the empirical gap grows, Stokes points become depleted around small phases and concentrate on very large ones. This supports the idea that around the gapped minima, Stokes points will be concentrated at phases that are nearly $180°$, where the two-replica calculation shows that almost all of their nearest neighbors will lie.
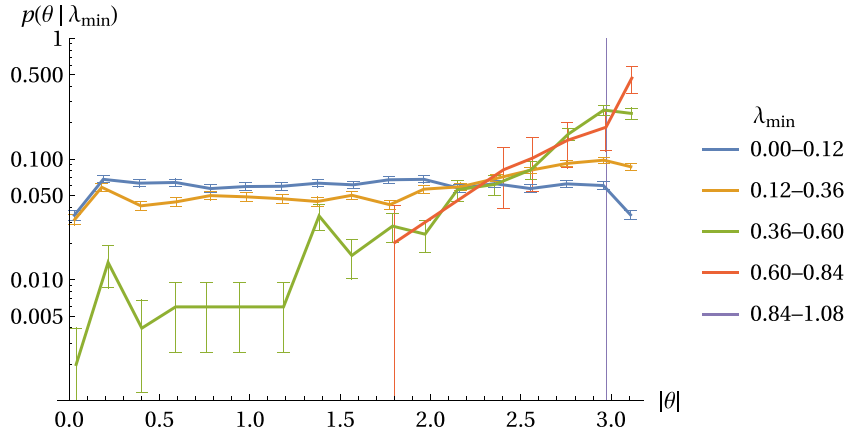
Figure 21. The probability density function for identified Stokes points as a function of $|\theta|$, the magnitude of the phase necessary to add to β to reach the Stokes point, at $N = 32$ and for several binned $|\lambda_{\min}|$. As the empirical gap is increased, the population of discovered Stokes points becomes more concentrated around $|\theta| = \pi$.

4.5. Pure p-spin: is analytic continuation possible?

After all this work, one is motivated to ask: can analytic continuation be done in even a simple complex model like the pure p-spin? Numeric and analytic evidence indicates that the project is hopeless if ungapped stationary points take a significant weight in the partition function, since for these Stokes lines proliferate at even small continuation and there is no hope of tracking them. However, for gapped stationary points we have seen compelling evidence that suggests they will not participate in Stokes points, at least not until a large phase rotation of the parameter being continued. This gives some hope for continuation of the low-temperature thermodynamic phase of the p-spin, where weight is concentrated in precisely gapped minima.

Recalling our expression (32) for the single-thimble contribution to the partition function expanded to lowest order in large $|\beta|$, we can write for the p-spin after an infinitesimal rotation of β into the complex plane (before any Stokes points have been encountered):

$$
\begin{aligned}
Z &= \sum_{\sigma \in \Sigma_0} n_\sigma Z_\sigma \\
&\simeq \sum_{\sigma \in \Sigma_0} \left(\frac{2\pi}{\beta} \right)^{D/2} i^{k_\sigma} |\det \text{Hess}\, \mathcal{S}(s_\sigma)|^{-\frac{1}{2}} e^{-\beta \mathcal{S}(s_\sigma)} \\
&\simeq \sum_{k=0}^{D} \int d\epsilon\, \mathcal{N}_{\text{typ}}(\epsilon, k) \left(\frac{2\pi}{\beta} \right)^{D/2} i^k |\det \text{Hess}\, \mathcal{S}(\epsilon, k)|^{-\frac{1}{2}} e^{-\beta N\epsilon},
\end{aligned}
\tag{99}
$$

where $\mathcal{N}_{\text{typ}}(\epsilon, k)$ is the typical number of stationary points in a sample of the real p-spin model in the energy range ε to $\epsilon + d\epsilon$ and with index k. Following Derrida [17], this is related to the *average* number of stationary points in this range at large N by:

$$
\mathcal{N}_{\text{typ}}(\epsilon, k) = \overline{\mathcal{N}}(\epsilon, k) + \eta(\epsilon, k) \overline{\mathcal{N}}(\epsilon, k)^{1/2},
\tag{100}
$$

where η is a random, sample-dependant number of order one. This gives two terms to the typical partition function:

$$
Z_{\text{typ}} = Z_A + Z_B,
\tag{101}
$$

where

$$Z_A \simeq \sum_{k=0}^{D} \int d\epsilon\, \overline{\mathcal{N}}(\epsilon,k) \left(\frac{2\pi}{\beta}\right)^{D/2} i^k |\det \text{Hess}\, \mathcal{S}(\epsilon,k)|^{-\frac{1}{2}} e^{-\beta N \epsilon} = \int d\epsilon\, e^{N f_A(\epsilon)} \quad (102)$$

$$Z_B \simeq \sum_{k=0}^{D} \int d\epsilon\, \eta(\epsilon,k) \overline{\mathcal{N}}(\epsilon,k)^{1/2} \left(\frac{2\pi}{\beta}\right)^{D/2} i^k |\det \text{Hess}\, \mathcal{S}(\epsilon,k)|^{-\frac{1}{2}} e^{-\beta N \epsilon} \quad (103)$$

$$= \int d\epsilon\, \tilde{\eta}(\epsilon) e^{N f_B(\epsilon)}, \quad (104)$$

for functions f_A and f_B defined by:

$$f_A = -\beta\epsilon + \Sigma(\epsilon) - \frac{1}{2} \int d\lambda\, \rho(\lambda \mid \epsilon)|\lambda| + \frac{1}{2}\log\frac{2\pi}{\beta} + i\frac{\pi}{2} P(\lambda < 0 \mid \epsilon) \quad (105)$$

$$f_B = -\beta\epsilon + \frac{1}{2}\Sigma(\epsilon) - \frac{1}{2} \int d\lambda\, \rho(\lambda \mid \epsilon)|\lambda| + \frac{1}{2}\log\frac{2\pi}{\beta} + i\frac{\pi}{2} P(\lambda < 0 \mid \epsilon), \quad (106)$$

and where $P(\lambda < 0 \mid \epsilon)$ is the cumulative probability distribution of the eigenvalues of the spectrum given ε,

$$P(\lambda < 0 \mid \epsilon) = \int_{-\infty}^{0} d\lambda'\, \rho(\lambda' \mid \epsilon), \quad (107)$$

and produces the macroscopic index k/N. Each integral will be dominated by its value near the maximum of the real part of the exponential argument. Assuming that $\epsilon < \epsilon_{\text{th}}$, this maximum occurs at:

$$0 = \frac{\partial}{\partial\epsilon} \text{Re} f_A \bigg|_{\epsilon=\epsilon_{\max}} = -\text{Re}\,\beta - \frac{1}{2}\frac{3p-4}{p-1}\epsilon_{\max} + \frac{1}{2}\frac{p}{p-1}\sqrt{\epsilon_{\max}^2 - \epsilon_{\text{th}}^2}, \quad (108)$$

$$0 = \frac{\partial}{\partial\epsilon} \text{Re} f_B \bigg|_{\epsilon=\epsilon_{\max}} = -\text{Re}\,\beta - \epsilon_{\max}. \quad (109)$$

As with the 2-spin model, the integral over ε is oscillatory and can only be reliably evaluated with a saddle point when either the period of oscillation diverges *or* when the maximum lies at a cusp. We therefore expect changes in behavior when $\epsilon_{\max} = \epsilon_{k=0}$, the ground state energy. The temperature at which this happens is:

$$\text{Re}\,\beta_A = -\frac{1}{2}\frac{3p-4}{p-1}\epsilon_{k=0} + \frac{1}{2}\frac{p}{p-1}\sqrt{\epsilon_{k=0}^2 - \epsilon_{\text{th}}^2} \quad (110)$$

$$\text{Re}\,\beta_B = -\epsilon_{k=0}, \quad (111)$$

which for all $p \geqslant 2$ has $\text{Re}\,\beta_A \geqslant \text{Re}\,\beta_B$. Therefore, the emergence of zeros in Z_A does not lead to the emergence of zeros in the partition function as a whole, because Z_B still produces a coherent result (despite the unknown constant factor $\tilde{\eta}(\epsilon_{k=0})$). It is only at $\text{Re}\,\beta_B = -\epsilon_{k=0}$ where both terms contributing to the partition function at large N involve incoherent integrals near the maximum, and only here where the density of zeros is expected to become nonzero.

In fact, in the limit of $|\beta| \to \infty$, $\text{Re}\,\beta_B$ is precisely the transition found in [9] between phases with and without a density of zeros, plotted in figure 22. This value is an underestimate for the transition for finite $|\beta|$, which likely results from the invalidity of our large-β approximation. More of the phase diagram might be constructed by continuing the series for individual thimbles to higher powers in β, which would be equivalent to allowing non-constant terms in the Jacobian of the coordinate transformation over the thimble.

This zeroth-order analysis for the p-spin suggests that analytic continuation can be sometimes done despite the presence of a great many complex stationary points. In particular, when
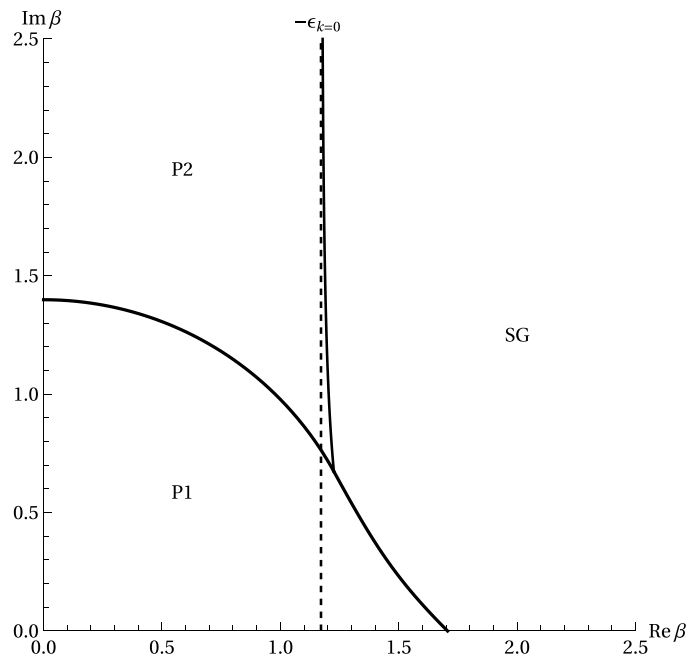
Figure 22. Phases of the 3-spin model in the complex-β, following Obuchi and Takahashi [9]. The phase P2 contains a nonzero density of zeros of the partition function, while the 'spin-glass' phase SG does not. Analytic continuation via thimbles correctly predicts the boundary between these two phases when $|\beta| \gg 1$ to be $\operatorname{Re}\beta = -\epsilon_0$, shown with a dashed line.

weight is concentrated in certain minima Stokes lines do not appear to interrupt the proceedings. How bad the situation is in other regimes, like for smaller $|\beta|$, remains to be seen: our analysis cannot tell between the effects of Stokes points changing the contour and the large-$|\beta|$ saddle-point used to evaluate the thimble integrals. Taking the thimbles to the next order in β may reveal more explicitly where Stokes points become important.

5. Conclusion

We have reviewed the Picard–Lefschetz technique for analytically continuing integrals and examined its applicability to the analytic continuation of configuration space integrals over the pure p-spin models. The evidence suggests that analytic continuation is possible when weight is concentrated in gapped minima, who seem to avoid Stokes points, and is likely intractable otherwise.

This has implications for the ability to analytically continue other types of theories. For instance, *marginal* phases of glasses, spin glasses, and other problems are characterized by concentration in pseudogapped minima. Based on the considerations of this paper, we suspect that analytic continuation is never tractable in such a phase, as Stokes points will always proliferate among even the lowest minima.

It is possible that a statistical theory of analytic continuation could be developed in order to treat these cases, whereby one computes the average or typical rate of Stokes points as a function of stationary point properties, and treats their proliferation to complex saddles as a

structured diffusion problem. This would be a very involved calculation, involving counting classical trajectories with certain boundary conditions, but in principle it could be done as in [15]. Here the scale of the proliferation may rescue things, allowing accurate statements to be made about its average effect.

Data availability statement

The data that support the findings of this study are available upon reasonable request from the authors.

Acknowledgment

ORCID iD

Jaron Kent-Dobias https://orcid.org/0000-0002-2163-5609

References

[1] Witten E 2011 Analytic continuation of Chern–Simons theory *Chern–Simons Gauge Theory: 20 Years After* (*AMS/IP Studies in Advanced Mathematics* vol 50) ed J E Andersen, H U Boden, A Hahn and B Himpel (Providence, RI: American Mathematical Society) pp 347–446

[2] Alexandru A, Başar G, Bedaque P F and Warrington N C 2022 Complex paths around the sign problem *Rev. Mod. Phys.* **94** 015006

[3] Howls C J 1997 Hyperasymptotics for multidimensional integrals, exact remainder terms and the global connection problem *Proc. R. Soc.* A **453** 2271–94

[4] Takagi T 1924 On an algebraic problem related to an analytic theorem of Carathéodory and Fejér and on an allied theorem of Landau *Jpn. J. Math.: Trans. Abstr.* **1** 83–93

[5] Nguyen H H and O'Rourke S 2014 The elliptic law *Int. Math. Res. Not.* **2015** 7620–89

[6] Kent-Dobias J and Kurchan J 4 2021 Complex complex landscapes *Phys. Rev. Res.* **3** 023064

[7] Livan G, Novaes M and Vivo P 2018 *Introduction to Random Matrices* (*SpringerBriefs in Mathematical Physics* vol 26) (Cham: Springer International Publishing)

[8] Weyl H 12 1912 Das asymptotische verteilungsgesetz der eigenwerte linearer partieller differentialgleichungen (mit einer anwendung auf die theorie der hohlraumstrahlung) *Math. Ann.* **71** 441–79

[9] Obuchi T and Takahashi K 3 2012 Partition-function zeros of spherical spin glasses and their relevance to chaos *J. Phys. A: Math. Theor.* **45** 125003

[10] Takahashi K and Obuchi T 2013 Zeros of the partition function and dynamical singularities in spin-glass systems *J. Phys.: Conf. Ser.* **473** 012023

[11] Auffinger A, Arous G B and Černý J 2012 Random matrices and complexity of spin glasses *Commun. Pure Appl. Math.* **66** 165–201

[12] Castellani T and Cavagna A 2005 Spin-glass theory for pedestrians *J. Stat. Mech.* P05012

[13] Kurchan J 1992 Supersymmetry in spin glass dynamics *J. Physique* I **2** 1333–52

[14] Etienne B 1779 *Théorie Générale des Équations Algbriques* (Paris: L'imprimerie de Ph.-D. Pierres, rue S. Jacques)

[15] Ros V, Biroli G and Cammarota C 2021 Dynamical instantons and activated processes in mean-field glass models *SciPost Phys.* **10** 002

[16] Folena G, Franz S and Ricci-Tersenghi F 2020 Rethinking mean-field glassy dynamics and its relation with the energy landscape: the surprising case of the spherical mixed *p*-spin model *Phys. Rev.* X **10** 031045

[17] Derrida B 9 1991 The zeroes of the partition function of the random energy model *Physica* A **177** 31–37